*This is a previous version of the article published in Neuroscience. 2020, 439: 62-79. https://doi.org/10.1016/j.neuroscience.2019.05.043*

# Mechanisms of blockade of the muscle-type nicotinic receptor by benzocaine, a permanently uncharged local anesthetic.

Raúl Cobo[a], Magdalena Nikolaeva[b], Armando Alberola-Die[a], Gregorio Fernández-Ballester[b], José Manuel González-Ros[b], Isabel Ivorra[a] and Andrés Morales[a,*]

([a]) División de Fisiología, Departamento de Fisiología, Genética y Microbiología, Universidad de Alicante, Apdo. 99, E-03080 Alicante, Spain.

([b]) Instituto de Investigación, Desarrollo e Innovación en Biotecnología Sanitaria de Elche (IDiBE), Universidad Miguel Hernández, Elche, E-03202, Alicante, Spain.

(*) Correspondence:

Andrés Morales

andres.morales@ua.es

Phone: +34-965903949

**Running title:**

Mechanisms of nAChR inhibition by benzocaine

**Abstract**

Most local anesthetics (LAs) are amine compounds bearing one or several phenolic rings. Many of them are protonated at physiological pH, but benzocaine (Bzc) is permanently uncharged, which is relevant because the effects of LAs on nicotinic acetylcholine (ACh) receptors (nAChRs) depend on their presence as uncharged or protonated species. The aims of this study were to assess the effects of Bzc on nAChRs and to correlate them with its binding to putative interacting sites on this receptor. nAChRs from *Torpedo* electroplaques were microtransplanted to *Xenopus* oocytes and currents elicited by ACh ($I_{ACh}$s), either alone or together with Bzc, were recorded at different potentials. Co-application of ACh with increasing concentrations of Bzc showed that Bzc reversibly blocked nAChRs. $I_{ACh}$ inhibition by Bzc was voltage-independent, but the $I_{ACh}$ rebound elicited when rinsing Bzc suggests an open-channel blockade. Besides, ACh and Bzc co-application enhanced nAChR desensitization. When Bzc was just pre-applied it also inhibited $I_{ACh}$, by blocking closed (resting) nAChRs. This blockade slowed down the kinetics of both the $I_{ACh}$ activation and the recovery from blockade. The electrophysiological results indicate that Bzc effects on nAChRs are similar to those of 2,6-dimethylaniline, an analogue of the hydrophobic moiety of lidocaine. Furthermore, docking assays on models of the nAChR revealed that Bzc and DMA binding sites on nAChRs overlap fairly well. These results demonstrate that Bzc inhibits nAChRs by multiple mechanisms and contribute to better understanding both the modulation of nAChRs and how LAs elicit some of their clinical side effects.

**Keywords:**

*Xenopus* oocytes, desensitization, open-channel blockade, closed-channel blockade, rebound currents, virtual-docking assays.

**Abbreviations:**

ACh, acetylcholine; ANR, normal Ringer solution with atropine; Bzc, benzocaine; CI, confidence interval; DEA, diethylamine; DMA, 2,6-dimethylaniline; EC, extracellular; $GABA_AR$, gamma-aminobutyric acid (GABA) receptor type A; $I_{ACh}$, ACh-elicited current; IC, intracellular; $I_{GABA}$, GABA-elicited current; $I_p$, $I_{ACh}$ amplitude at the peak; $I_{Rb}$, $I_{ACh}$ rebound current; $I_{ss}$, $I_{ACh}$ amplitude at the steady-state; LA, local anesthetic; LGIC, ligand-gated ion channel; Lid, lidocaine; MS-222, ethyl 3-aminobenzoate methanesulfonate; n, number of oocytes; N, number of oocyte-donor frogs; nAChR, nicotinic acetylcholine receptor; RMSD, root-mean-square deviation; SEM, standard error of the mean; TM, transmembrane spanning-segment; Ttc, tetracaine.

**Highlights:**

- Nicotinic acetylcholine receptors (nAChRs) from *Torpedo* electroplax were microtransplanted to the *Xenopus* oocyte membrane.
- Benzocaine elicited multiple inhibitory actions on muscle-type nAChRs, including open- and closed-channel blockade.
- Desensitization of nAChRs was boosted by benzocaine.
- Benzocaine gave raise to marked rebound currents after its co-application with acetylcholine.
- Binding of benzocaine to the nAChR mimicked that of 2,6-dimethylaniline, an analogue of the hydrophobic moiety of lidocaine.

## INTRODUCTION

The main target of local anesthetics (LAs) is the voltage-dependent $Na^+$ channel, promoting its blockade and favoring the inactivated state (Hille, 1966; Catterall and Mackie, 2001; Fukuda *et al.*, 2005), thus preventing the generation of action potentials in nerve cells. Besides, most LAs interact with other ion channels, including ligand-gated ion channels (LGIC), as the nicotinic acetylcholine (ACh) receptor (nAChR). Therefore, it is of therapeutic relevance to understand the mechanisms by which LAs modulate nAChRs and other LGIC, since these interactions might account for some of the effects found when LAs are used in the clinical practice.

The muscle-type nAChRs belong to the "Cys-loop" family of receptors, which are involved in fast synaptic transmission. They are densely packed at the postsynaptic membranes of both skeletal muscle fibers and electrocytes of some electric fishes, as *Torpedo*. These nAChRs are pentameric ensembles composed of $2\alpha_1$, $1\beta_1$, $1\delta$ and either $1\varepsilon$ or $1\gamma$ subunits, assembled to shape a central channel pore. The ε-subunit is present in nAChRs located at the neuromuscular junction during the postnatal life (junctional-type receptors) and is equivalent to the γ-subunit from *Torpedo* nAChRs; however, embryonic and extrajunctional nAChRs from muscle fibers express a different γ-subunit (extrajunctional-type receptors) (Albuquerque *et al.*, 2009; Sine, 2012; Bouzat and Mukhtasimova, 2018). Neuronal nAChRs are also pentameric, but they show a larger heterogeneity in subunit composition and stoichiometry, despite they only express α ($\alpha_2$-$\alpha_{10}$) and β ($\beta_2$- $\beta_4$) subunits (Albuquerque *et al.*, 2009, Hurst *et al.*, 2013). This large diversity of nAChR structural conformation is of great relevance since it accounts for a plethora of functional and pharmacological properties of nAChRs. The structural conformation of muscle-type nAChRs has been mainly unraveled thanks to the pioneering work of Nigel Unwin, who used high-resolution electron microscopy on 2-D crystals of *Torpedo* electroplax membranes to determine the nAChR structure in the closed (Toyoshima and Unwin, 1988; Unwin, 2005) and open (Unwin, 1995; Unwin and Fujiyoshi, 2012) states. The resulting structural models have paved the way to carry out "*in silico*" studies addressed to improve the knowledge, at a molecular scale, of nAChR function and modulation. Recently, Newcombe *et al.* (2018) found some inaccuracies in the transmembrane domain (TMD) alignment of the *Torpedo* nAChR structure, mainly involving a shift of one helix turn at the base of the M1-M2 helices and these authors corrected this misalignment for the homomeric $\alpha_7$ nAChR.

From the last few decades, it is well known that some LAs modulate nAChR function at the end-plate (Steinbach, 1968; Kordas, 1970; Deguchi and Narahashi, 1971; Katz and Miledi, 1975). Later on, it was found that certain LAs, or their derivatives with positively-charged quaternary-ammonium groups, bind into the nAChR channel pore, eliciting open-channel blockade, as referred for the lidocaine (Lid) derivatives QX-222 and QX-314 (Neher and Steinbach, 1978; Pascual and Karlin, 1998), procaine (Adams, 1977), Lid (Alberola-Die *et al.*, 2011), diethylamine (DEA), which resembles the hydrophilic moiety of Lid (Alberola-Die *et al.*, 2016a) or tetracaine (Ttc; Cobo *et al.*, 2018). Nevertheless, most LAs are amphipathic molecules, containing an aromatic ring and an amine group and, therefore, at physiological solutions, most of them are present both as charged and uncharged forms. Hence, most LAs are able to bind to different nAChR residues, mainly located at the extracellular- and transmembrane-domains (ECD and TMD, respectively), as we have previously reported for Lid (Alberola-Die el al., 2016a) and Ttc (Cobo *et al.*, 2018). Actually, this heterogeneity in nAChR binding sites for Lid, and other LAs, accounts for their multiple inhibitory actions on these receptors (Alberola-Die *et al.* 2011). Furthermore, most Lid actions could be fairly well mimicked by small molecules resembling either its hydrophilic fraction, as the positively charged DEA (Alberola-Die *et al*., 2016a), or its hydrophobic moiety, as the uncharged 2,6-dimethylaniline (DMA, Alberola-Die *et al*., 2016b). Though most LAs, or their derivatives, seem to act on nAChRs by similar blocking mechanisms, as open-channel blockers, there are pronounced differences in their potency as nAChR inhibitors, differing in several orders of magnitude. Moreover, some LAs show additional effects on nAChRs, as the blockade of resting nAChRs, elicited by either Lid (Alberola-Die *et al.*, 2011) or Ttc (Middleton *et al.*, 1999; Cobo *et al.*, 2018), or the enhancement of desensitization, caused by adiphenine (Spitzmaul *et al.*, 2009), Lid (Alberola-Die *et al.*, 2011) or Ttc (Cobo et al, 2018). Noticeably, these later effects of LAs on nAChRs are usually elicited at concentrations higher than those required to cause the open-channel blockade.

Benzocaine (Bzc) is a hydrophobic LA widely used in clinical practice, mainly to relieve mild dental and dermatological pain (González-Rodríguez *et al.*, 2013). As well as for other LAs, the main target of Bzc are voltage-gated $Na^+$ channels, but it includes also other membrane proteins, including *Torpedo* nAChRs (Mantipragada *et al.*, 2003)

or the Ca-ATPase of the sarcoplasmic reticulum (Di Croce *et al.*, 2015), and thus modifies their function. We have now studied the structural and functional interaction of Bzc (see chemical structure in the inset to Fig. 1B) on muscle-type nAChRs. The $pk_a$ of Bzc is 2.78 (data from Chemicalize, https://chemicalize.com/) and, therefore, less than 1 in 10.000 molecules of Bzc are in a charged form at the recording pH. Interestingly, in spite of being an uncharged molecule, it has been reported that Bzc elicits voltage-independent blockade of nAChRs by acting into the open channel pore (Ogden *et al.*, 1981). Therefore, the present work was aimed, first, to ascertain the mechanisms by which Bzc modulates muscle-type nAChR function and, second, to decipher the nAChR sites at which Bzc binds to mediate its actions. Our results confirm that Bzc blocks nAChRs by acting within the channel-pore, but also blocks resting nAChRs and promotes their desensitization at concentrations close to its $IC_{50}$. In addition, the functional effects of Bzc on nAChRs have been correlated to its binding at specific sites on the nAChR, determined by docking assays, using structural models of *Torpedo* nAChR, both in the closed and the open states, as templates.

Preliminary results of this work have been published elsewhere in an abstract form (Cobo *et al*., 2016).

## EXPERIMENTAL PROCEDURES

### Oocyte microinjection with proteoliposomes bearing either nAChRs or $GABA_A$Rs

*Torpedo marmorata* nAChRs were purified and reconstituted in asolectin lipids, at a final protein concentration of 0.3-1.2 mg/mL, as previously reported (Ivorra *et al.*, 2002). Adult female *Xenopus laevis* (purchased from Centre National de la Recherche Scientifique, Montpellier, France) were immersed in cold 0.17% tricaine methanesulfonate (MS-222) for 20 min and a piece of ovary was drawn out aseptically. Animal handling was carried out in accordance with the guidelines for the care and use of experimental animals adopted by the European Union (European Communities Council Directive of 24 November 1986, 86/609/EEC), and the animal protocol was approved by the Ethic Committee of Universidad de Alicante. Stage V and VI oocytes were isolated and their surrounding layers removed manually. Cells were kept at 15-16ºC in a modified Barth's solution (88 mM NaCl, 1 mM KCl, 2.40 mM $NaHCO_3$, 0.33 mM $Ca(NO_3)_2$, 0.41 mM $CaCl_2$, 0.82 mM $MgSO_4$, 10 mM HEPES (pH 7.4), 100 U/mL

penicillin and 0.1 mg/mL streptomycin) until used. Oocytes were microinjected with 100 nL of an aliquot of reconstituted nAChRs (Morales *et al.*, 1995).

In some experiments, gamma-aminobutyric acid (GABA) receptors ($GABA_A$Rs) were microtransplanted to the *Xenopus* oocyte membrane from rat-brain synaptosomal-enriched membranes, as previously described (Alberola-Die *et al.*, 2016a). Briefly, whole rat brains were removed and homogenized in a glass-Teflon homogenizer in 10 volumes of ice-cold 10 mM Tris-citrate buffer (pH 7.4) containing 300 mM sucrose, 1 mM EDTA, 1 mM EGTA and 500 μM PMSF. Each homogenate was spun at 1000 × g for 10 min and the supernatant centrifuged at 45,000 × g for 30 min (4°C). Pellet was resuspended in 5 mL of 50 mM Tris-citrate (pH 7.4) containing 1 mM EDTA and 1 mM EGTA and 500 μM PMSF, frozen in liquid $N_2$ for 5 min and then thawed for 20 min at 20°C in an ultrasonic bath. Suspension was spun 30 min (4°C) at 45,000 × g. The final pellet was resuspended in 50 mM Tris-citrate buffer in 1:10 mass/volume ratio and protein concentration assayed (Pierce kit, Pierce Chem. Co., Rockford, IL, USA). Samples containing 1-3 mg/mL of protein were aliquoted and kept at -80ºC for later use.

**Two-electrode voltage-clamp recordings in oocytes**

Membrane current recordings were performed at 21-25 ºC, 16-72 h after proteoliposome injection, as previously reported (Morales *et al.*, 1995; Alberola-Die *et al.*, 2016b). Briefly, oocytes were placed in a 150 μL recording chamber and continuously superfused with normal frog Ringer's solution (115 mM NaCl, 2 mM KCl, 1.8 mM $CaCl_2$, 5 mM HEPES, pH 7.0) supplemented with 0.5 μM atropine sulfate (normal Ringer with atropine, ANR) to block any muscarinic response (Kusano *et al.*, 1982). The membrane potential was held at -60 mV, unless otherwise stated. Oocytes were superfused with ACh either alone or together with Bzc at a flow rate of 13-17 mL/min. Membrane currents elicited by ACh ($I_{ACh}$) either alone or co-applied with Bzc, were low-pass filtered at 30-1000 Hz and, after sampling at fivefold the filter frequency (Digidata series 1440A and 1550; Axon Instruments, Foster City, CA, USA), recorded on two PC-computers, using the WCP v. 4.8.6 package developed by J. Dempster (Strathclyde Electrophysiology Software, University of Strathclyde, Scotland, UK) and AxoScope v. 10.0.0.60 (Molecular Devices Corporation, Sunnyvale, CA, USA).

**Experimental design**

Experimental procedures were similar to those used to study the Lid and Ttc effects (Alberola-Die *et al*., 2011; Cobo *et al*., 2018) on nAChRs. Briefly, Bzc concentration-$I_{ACh}$ inhibition relationship was determined by measuring $I_{ACh}$s evoked by 10 μM ACh alone or together with different Bzc concentrations. For competition assays, ACh concentration-$I_{ACh}$ amplitude curves were obtained by bathing injected oocytes with increasing ACh concentrations either alone or together with 500 μM Bzc. $I_{ACh}$s were normalized to the maximum $I_{ACh}$ evoked by ACh alone or in the presence of Bzc, and the values fitted to a sigmoid curve (see equation 4 below). To allow nAChRs to recover from desensitization, the interval between consecutive ACh applications was at least 5 min. To assess the blockade of resting nAChRs by Bzc, we compared the $I_{ACh}$s elicited by ACh (from 3 μM to 1 mM) alone, or co-applied with 500 μM Bzc, either directly, or after 12 s of Bzc pre-application (same concentration). In some oocytes, a 20 s application of Bzc was given during the $I_{ACh}$ plateau elicited by either 10 or 100 μM ACh, in order to determine the time course of the open-channel blockade by Bzc and the recovery from it. To better characterize the rebound currents ($I_{Rb}$s) elicited by Bzc, in some experiments, the oocyte remained superfused with Bzc, for 12 s, after withdrawal of 100 μM ACh. The voltage-dependence of the $I_{ACh}$ blockade by Bzc was assessed by applying series of 800 ms voltage pulses (from -120 to +60 mV, in 20 mV steps) to the oocyte before ligand superfusion and during the $I_{ACh}$ plateau elicited by 10 μM ACh, either alone or co-applied with 500 μM Bzc. The -120 mV pulse duration was extended up to 1500 ms to allow a more complete current relaxation.

Oocytes previously injected with synaptosomal membranes bearing $GABA_AR$ were superfused with 1 mM GABA alone or together with Bzc (500 μM - 1 mM) to assess the Bzc effects on GABA elicited currents ($I_{GABA}$).

**Data analysis and statistical procedures**

Inhibition curves were determined by measuring the $I_{ACh}$ evoked by 10 μM ACh in the presence of different concentrations of Bzc. The $I_{ACh}$s (both at the peak, $I_p$, and 20 s later, $I_{ss}$) elicited in the presence of Bzc were normalized to the $I_{ACh}$ evoked by ACh alone. Data were fitted to a logistic curve with the Origin 6.1 software (OriginLab Corp. Northampton, MA, U.S.A.), using the following equation (1):

$$I_{ACh+Bzc} = \left( \frac{I_{ACh}max - I_{ACh}min}{1 + ([Bzc]/IC_{50})^{n_H}} \right) + I_{ACh}min$$

where $I_{ACh+Bzc}$ is the $I_{ACh}$ amplitude elicited by co-application of 10 µM ACh with Bzc at a given concentration ([Bzc]); $I_{ACh}max$ and $I_{ACh}min$ are the maximum and minimum $I_{ACh}$s recorded, respectively; $IC_{50}$ is the Bzc concentration required to inhibit half the $I_{ACh}max$; and $n_H$ is the Hill coefficient.

The rate of desensitization ($I_{ACh}$ decay) was determined by measuring the $I_{ACh}$ amplitude elicited by 100 µM ACh, either alone or co-applied with 500 µM Bzc, at different times after $I_p$. Desensitization rates were computed using the equation (2):

$$D_{ti} = [1 - (I_{ti}/I_p)] \times 100$$

where $D_{ti}$ is the desensitization value at 2, 10 or 20 s after $I_p$; and $I_{ti}$ the remaining $I_{ACh}$ after the specified times (Olivera-Bravo *et al.*, 2007). In addition, based on the methods of Sobolevsky *et al*. (1999), the change in the rate of desensitization induced by 500 µM Bzc was determined using the following equation (3):

$$I_{ACh}\ desensitization\ change = \left( \frac{I_{ss\_Bzc}/I_{p\_Bzc}}{I_{ss\_Ctr}/I_{p\_Ctr}} \right)$$

where $I_{p\_Ctr}$ and $I_{p\_Bzc}$ are the $I_{ACh}$ peaks elicited by ACh either alone or together with Bzc, respectively; $I_{ss\_Ctr}$ and $I_{ss\_Bzc}$ are $I_{ACh}$s 20 s after the corresponding $I_p$s. The apparent time-to-peak was determined as the time elapsed from $I_{ACh}$ onset to the $I_p$, from currents elicited by ACh either alone or with Bzc. We have called this parameter as "apparent" time-to-peak, just to indicate that these values do not necessarily reflect "real" time-to-peak values of nAChR activation but those observed in our experimental conditions.

To characterize the pharmacological profile of nAChR blockade by Bzc, nAChRs were activated by different concentrations of ACh alone, or co-applied with Bzc, at roughly its $IC_{50}$, either directly, or after its pre-application for 12 s. Dose-response data were fitted to the following form of the Hill equation (4):

$$I/I_{Ach}max = [1 + (EC_{50}/[ACh])^{n_H}]^{-1}$$

where $I$ is the $I_{ACh}$ amplitude elicited at a given concentration of ACh ([ACh]) applied either alone, or together with Bzc; $EC_{50}$ is the agonist concentration required to obtain one-half the maximum $I_{ACh}$; and $I_{ACh}max$ and $n_H$ are as in equation 1.

Net *i/v* curves for $I_{ACh}$ were obtained by subtracting, for each voltage, the steady-state currents attained in ANR (measured during the last 100 ms of the pulse) from the corresponding currents recorded in the presence of 10 µM ACh alone or together with Bzc. These net $I_{ACh}$ values were normalized, for each oocyte, to the ACh response at -60 mV.

To determine the rate of open-channel blockade by Bzc, the oocyte was superfused with 500 µM Bzc at the plateau of the $I_{ACh}$ elicited by 10 or 100 µM ACh. Then, the $I_{ACh}$ decrease elicited by Bzc was fitted to a single exponential function. The time constant ($\tau$) of the $I_{ACh}$ decay was computed by using the OriginPro 8 software (OriginLab Corp. Northampton, MA, U.S.A.). The same procedure was used to determine the kinetics of $I_{ACh}$ recovery upon Bzc withdrawal.

Unless otherwise specified, values presented were the mean ± standard error of the mean (SEM); "*n*" indicates the number of oocytes and "*N*" is the number of oocyte-donor frogs from which the data were obtained. When comparing two-group means of normally distributed values, the Student's *t*-test was used; otherwise, the Mann-Whitney rank-sum test was applied. Among-group differences were determined by the analysis of variance (ANOVA), and mean differences for each pair of groups were determined with the Bonferroni *t*-test. The one-sample *t*-test was used to compare the mean of an experimental group with a specified value. For the comparison of $EC_{50}$ and $IC_{50}$ values, we used the confidence intervals (CIs) computed by the curve-fitting function of the Origin 6.1 software, using 95% confidence levels. The criterion of "non-overlapping 95% confidence intervals" was used to determine significant differences. A significance level of $p < 0.05$ was considered in all cases.

## Virtual docking assays

### *Refined nAChR structural model*

As mentioned above, the *Torpedo* nAChR structures in the open and closed states from Unwin models (pdb 4AQ9 and 2BG9, respectively; Unwin 1995, 2005) were recently demonstrated inaccurate at the TMD level (Newcombe *et al.* 2018). These authors refined the structural models for the $\alpha_7$ subunit (open and closed states), but not for the different subunits conforming the muscle-type nAChR. Therefore, all *Torpedo* subunits have been now modelled by homology using the rectified $\alpha_7$ subunit, both in the open

and the closed states. Sequences of *Torpedo* subunits were obtained from Uniprot database (https://www.uniprot.org/) having the codes P02711 (alfa), Q6S3I0 (beta); Q6S3H9 (gamma), and Q6S3H8 (delta). Sequence alignments were done with Clustal Omega (Sievers *et al.* 2011) from the European Bioinformatics Institute site (https://www.ebi.ac.uk/Tools/msa/clustalo/). The alignments were supervised to ensure that all TMDs aligned well with the template. The homology modeling was performed using the Swiss-Model Protein Modeling Server (Schwede *et al.* 2003) on the ExPASy Molecular Biology website (http://kr.expasy.org/) under the Project Mode. Structure visualization and modifications were made using Yasara v18.11.10 (Krieger *et al.* 2002) and DeepView v4.1 (Guex and Peitsch 1997). The orientation and optimization of the side chains were energy minimized using Yasara (http://www.yasara.org). Briefly, this process involved an initial short steepest descent minimization to remove bumps, followed by a simulated annealing minimization. In this procedure, the simulation cell was slowly cooled towards 0º K by downscaling the atom velocities. The entire system was subjected to an equilibration process before a short molecular dynamics simulation. The equilibration consisted of an initial minimization of the fixed backbone atoms. Then, the restrained carbon alpha atoms were minimized and a 10 ps molecular dynamics optimization was performed to reduce the initial incorrect contacts and to fill the empty cavities. Finally, under periodic boundary conditions in the three coordinate directions, the full system was simulated at 310º K for 0.5 ns. All dynamic simulations were performed using Yasara (Krieger *et al.*, 2002) with the force field AMBER03 (Duan *et al*., 2003). The cutoff used for long-range interactions was set at 10 Å. In addition, the model was evaluated using PROCHECK to show the residues in the allowed regions of the Ramachandran plots (Laskowski *et al.*, 1996).

The pentameric organization of the *Torpedo* nAChR channel was accomplished by superposition of the different subunits (either in the open or closed states) on cryo-electron microscopy structures (pdb 4AQ9 & 2BG9). Yasara was used for superimpositions, obtaining a maximum of 4.4 Å of root-mean-square deviation (RMSD) over 2708 matched atoms. The final rectified open and closed pentamers of *Torpedo* nAChR were energy minimized with Yasara (fixed backbone) to avoid intersubunit clashes.

***Bzc docking assays***

The structure of Bzc (PubChem CID: 2337) was obtained from the National Center for Biotechnology Information (NCBI) PubChem database (http://www.ncbi.nlm.nih.gov/pccompound). The docking procedure was as previously published (Alberola-Die, et al, 2016a, b; Cobo et al, 2018). Briefly, the global docking procedure was accomplished with AutoDock 4 (Morris *et al.*, 2008) implemented in Yasara, in which a total of 800 flexible docking runs were set and clustered around the putative binding sites. The program then performed a simulated annealing optimization of the complexes, which moved the structure to a nearby stable energy minimum, by using the implemented Assisted Model Building with Energy Refinement (AMBER03) force field (Duan *et al.*, 2003). The Yasara pH command was set to 7.0, to ensure that molecules preserved their pH dependency of bond orders and protonation patterns. In this way, 99.9% of the Bzc molecules were unprotonated. The best binding energy complex in each cluster was stored, analyzed, and used to select the best orientation of the interacting partners.

The theoretical affinities of Bzc at its binding site were determined by calculating the binding energy of the ligand-receptor complex. The binding energy was obtained by measuring the energy at infinite distance (the unbound state) and subtracting from that value the energy of the complex at the bound state.

Figures were drawn with open source PyMol (The PyMOL Molecular Graphics System, Version 1.8 Schrödinger, LLC, at http://www.pymol.org/).

**Drugs**

ACh, atropine sulphate, Bzc, GABA, MS-222, DMSO, penicillin and streptomycin were from Sigma-Aldrich (St. Louis, MO, USA) and ethanol from Merck KGaA (Darmstadt, Germany). HEPES was obtained from Acros Organics (New Jersey, NJ, USA). Other reagents of general use were purchased from Scharlau Chemie SA (Barcelona, Spain). Bzc solutions were prepared from a 0.1 M stock solution in DMSO or, in a few cases, from a 0.5 M stock solution in ethanol. All solutions were made in ANR just before each application.

RESULTS

**Inhibition of $I_{ACh}$ by Bzc**

Superfusion of Bzc (up to 1 mM) to either uninjected oocytes or those bearing microtransplanted nAChRs, with the membrane potential held at -60 mV, had almost no effects on the cell membrane conductance. Nevertheless, at 300 µM or above, Bzc (diluted from a stock solution in either ethanol or DMSO) elicited a small and slow outward current in 25 out of 34 cells (74%). This current was most likely due to the blockade of native channels of the oocyte membrane, though we did not pursue this finding any further. In any case this small outward current (7.2 ± 0.9 nA; n = 25; N = 12) did not significantly affect the kinetics of the comparatively much larger $I_{ACh}$s (usually several hundreds of nA). Thus, for instance, the $I_{ACh}$ apparent time-to-peak in cells showing Bzc-induced outward current was not significantly different from that of oocytes lacking this current.

In microinjected oocytes, co-application of 10 µM ACh with 0.1 µM-2 mM Bzc reversibly reduced $I_p$, in a dose-dependent manner (Fig. 1A), following a sigmoid function (Fig. 1B). Over 300 µM Bzc, the extent of $I_{ACh}$ inhibition measured 20 s after $I_p$ ($I_{ss}$) was greater than that corresponding to $I_p$ values. Thus, the $IC_{50}$ and $n_H$ values (see equation 1) for the $I_p$ were 382 µM (CI, 305-487 µM; n = 3-20, N = 1-10) and 1.0 ± 0.2, respectively (Fig. 1B). The dose-inhibition curve for the $I_{ss}$ showed a lower $IC_{50}$ (220 µM, CI 179-251 µM, same cells and donor frogs as above) and a slope 1.2 ± 0.2 (Fig. 1B). Most likely, this lower $IC_{50}$ for $I_{ss}$ is because of an enhancement of nAChR desensitization by Bzc (see below).

The specificity of Bzc effects on muscle-type nAChR blockade was assessed by comparing its effects on $GABA_A$Rs, which belong to the same Cys-loop family of receptors. When Bzc (500 µM - 1 mM) was co-applied with GABA (1 mM) to oocytes microinjected with rat brain synaptosomal membranes bearing $GABA_A$Rs, $I_{GABA}$ decreased and the kinetics of the current decay was accelerated (Fig. 2), as it was found for muscle-type nAChRs.

**Voltage-dependence of nAChRs blockade by Bzc**

To unravel whether $I_{ACh}$ inhibition exerted by Bzc has voltage-dependence, voltage jumps (from -120 to +60 mV, in 20 mV steps) were imposed to oocytes while superfusing them with just ANR or during the $I_{ACh}$ plateau elicited by 10 µM ACh, either alone or together with 500 µM Bzc (Fig. 3A). The i/v curves of net $I_{ACh}$s elicited by ACh, either alone or co-applied with 500 µM Bzc, showed that the $I_{ACh}$ blockade by

Bzc was rather voltage independent (Fig. 3B). Nevertheless, when plotting the percentage of $I_{ACh}$ inhibition versus membrane potential a slight trend in voltage-dependence arises. Thus, at negative potentials, the more hyperpolarized the cell membrane, the larger $I_{ACh}$ blockade (Fig. 3C), though without significant differences at the different potentials tested ($p > 0.05$, ANOVA test). The lack of significant voltage dependence of the $I_{ACh}$ inhibition by Bzc contrasts with the effects on nAChRs of other LAs with more protonatable amine groups on nAChRs, as Lid (Alberola-Die *et al.*, 2011, 2013) or Ttc (Koblin & Lester, 1979; Cobo *et al.*, 2018). However, this lack of voltage-dependence does not exclude that Bzc might bind into the channel pore (see below). The i/v curves showed that the $I_{ACh}$ reversal potential, close to -5 mV, was not affected by the presence of Bzc.

**Competition assays**

To assess the pharmacological profile of nAChR inhibition by Bzc, oocytes were superfused with ACh at different concentrations (10, 100 µM and 1 mM) alone or co-applied with 500 µM Bzc either directly or following a 12 s pre-application of the same Bzc concentration. Furthermore, in some cells, 500 µM Bzc was pre-applied for 12 s to the oocyte prior to challenging the cell with ACh alone at the referred concentrations. Co-application of 10 µM ACh with 500 µM Bzc reduced $I_p$ roughly by half, as expected from the $IC_{50}$ value computed from the dose-inhibition curves (Fig. 1B). Under this experimental protocol, the percentage of $I_p$ inhibition was similar for any ACh concentration tested, suggesting that Bzc is acting as a non-competitive blocker, except for 100 µM ACh, which showed a slightly higher inhibition (56 ± 3 %, n = 18 versus 69 ± 3 %, n = 19 for 10 and 100 µM ACh, respectively; $p < 0.05$, ANOVA and Bonferroni *t*-test; Fig. 4$A_1$, $A_2$, $A_3$). Interestingly, the $I_p$ blockade increased when 500 µM Bzc was pre-applied and then co-applied with ACh. Thus, some of the nAChR blockage elicited by this protocol of Bzc application should be due to Bzc binding to resting (closed) nAChRs, preventing their activation by the agonist. Furthermore, pre- and co-application of Bzc slowed down the $I_{ACh}$ activation, and so the time needed to reach $I_p$ was markedly increased (Table 1; Fig. 4$A_1$, $A_2$, $A_3$). Noticeably, when Bzc was solely pre-applied before challenging the cell with ACh alone, i.e. Bzc only acting on resting nAChRs, the $I_p$ also decreased and $I_{ACh}$ activation slowed down, particularly at high ACh concentrations (Table 1 and Fig. 4$A_1$, $A_2$, $A_3$). This suggests that binding of Bzc to resting nAChRs disturbs the agonist binding, the channel gating or both events. Given

the effects of Bzc pre-application on $I_{ACh}$ activation, we quantified its inhibitory action on nAChRs only at the $I_{ss}$s, i.e. the $I_{ACh}$ amplitudes 20 s after its $I_p$ in the presence of Bzc. As shown in Fig. 4B, the extent of $I_{ss}$ inhibition was rather similar if Bzc was just co-applied with ACh or pre-applied and then co-applied with ACh. The percentage of $I_{ss}$ inhibition when co-applying 10 µM ACh with 500 µM Bzc was close to 80%, and this percentage increased significantly with the ACh concentration (Fig. 4B). This dependence on ACh concentration might be related to the enhancement of nAChR desensitization by Bzc (see below), which increases with ACh concentration. Interestingly, at 10 µM ACh, $I_{ss}$ decreased by roughly 25% when Bzc was just pre-applied, and this inhibitory effect was even more pronounced as the ACh concentration augmented. This indicates that Bzc is blocking resting (closed) nAChRs and that its recovery after rinsing the Bzc is very slow, particularly at high ACh concentrations (Fig. 4B).

**Rebound $I_{ACh}$s elicited by Bzc**

When oocytes bearing nAChRs are challenged with ACh at almost saturating concentrations (1 mM), an $I_{Rb}$ arises during the agonist washout (Fig. $4A_3$) because at these concentrations the ACh molecules by themselves plug the channel pore, eliciting open-channel blockade (Sine and Steinbach, 1984; Legendre *et al.*, 2000; Alberola-Die *et al.*, 2016b). Since ACh molecules are positively charged, this open-channel blockade is voltage-dependent, being only detected at negative potentials. Interestingly, co-application of Bzc, at its $IC_{50}$, with 100 µM ACh gave rise to pronounced $I_{Rb}$s (Fig. $4A_2$), whereas 100 µM ACh alone did not. Furthermore, if Bzc concentration was raised to 1 mM, $I_{Rb}$s were elicited even at 10 µM ACh (see Fig. 1A), which reminds what we previously found when co-applying DMA and ACh (Alberola-Die *et al.*, 2016b). To further explore the mechanisms involved in this $I_{Rb}$, oocytes were challenged with 100 µM ACh either alone or co-applied with 500 µM Bzc while the membrane potential was held either at -60 or +40 mV. Then we compared the $I_{Rb}$ amplitudes, normalized to their preceding $I_{ss}$ values, under two experimental conditions: **i)** washing out ACh and Bzc; and **ii)** removing ACh while Bzc still bathed the cell for 12 s. As indicated above, when $I_{ACh}$s were elicited by ACh alone, the agonist rinse elicited $I_{Rb}$ neither at -60 nor at +40 mV (Fig. $5A_1$, $A_2$). In contrast, washing ACh and Bzc out, after their co-application, evoked pronounced $I_{Rb}$s at both membrane potentials. The easiest explanation for these $I_{Rb}$s is the Bzc withdrawal from the channel pore while some ACh molecules are still

bound to the orthosteric site, since it has been found that Bzc, at these concentrations, binds inside the nAChR channel pore (Odgen *et al.*, 1981). Nevertheless, when ACh and Bzc co-application was followed by only ACh removal, i.e. the oocyte remained superfused with Bzc, $I_{Rb}$s still rose, both at -60 and at +40 mV. However, these $I_{Rb}$s were significantly smaller than those elicited when ACh and Bzc were withdrawn simultaneously (Fig. 5B). This is a rather unexpected result, since it suggests that the own ACh molecules are somehow contributing to these $I_{Rb}$s. Interestingly, the mechanism underlying the $I_{Rb}$*s* elicited by rinsing ACh alone should be different from open channel-blockade, because ACh is positively charged and these $I_{Rb}$s were found when holding the membrane potential both at -60 and at +40 mV (Fig. $5A_2$, B).

**Kinetics of nAChR blockade by Bzc and its recovery.**

As aforementioned, nAChR inhibition by Bzc involves both, open- and closed-channel blockade. To better understand how open nAChRs are blocked by Bzc, we tested the effect of a 20 s pulse of 500 µM Bzc applied during the $I_{ss}$ elicited by a 50 s pulse of either 10 or 100 µM ACh (Fig. $6A_1$, $A_2$). Co-application of ACh and Bzc evoked a fast and large inhibition of $I_{ss}$, being this blockade slightly higher at 100 µM ACh ($I_{ss}$ inhibition of 80 ± 2%, n= 9, and 88 ± 2%, n= 10, for 10 and 100 µM ACh, respectively; $p < 0.05$, *t*-test). However, the kinetics of this $I_{ACh}$ blockade was similar when Bzc was co-applied with either 10 or 100 µM ACh. The time constant obtained for the fast blockade phase, estimated by fitting the recordings to a single exponential function, was roughly 1.5 s, corresponding to the solution exchange kinetics (Fig. 6B; Cobo *et al.*, 2018). This indicates that the blockade of open nAChRs follows a faster kinetics, which we cannot resolve. In contrast, the recovery of nAChRs from Bzc blockade showed a slower time-course (Fig. 6B) and its kinetics was not limited by our solution exchange. Something similar was found when nAChRs were blocked by other LAs, as Lid (Alberola-Die *et al.*, 2011) or Ttc (Cobo *et al.*, 2018). Remarkably, the extent of $I_{ACh}$ recovery 15 s after washing out Bzc was significantly higher when Bzc was co-applied with 100 than with 10 µM ACh (Fig. 6C). The difference in the percentages of $I_{ACh}$ recovery when testing different ACh concentrations might be related to the different percentage of open nAChRs at these two ACh concentrations. In this sense, it should be pointed out that the kinetics of $I_{ACh}$ recovery from open-channel blockade is much faster than after closed-channel blockade, the latter lasting several decades of seconds, as evidenced by just Bzc pre-application (see Fig. $4A_1$, $A_2$, $A_3$).

**Bzc enhancement of nAChR desensitization**

At concentrations above 300 µM, Bzc accelerates $I_{ACh}$ decay, which results in a percentage of $I_{ss}$ inhibition higher than that of $I_p$ (Fig. 1A, B). This acceleration of $I_{ACh}$ decay by Bzc is similar to that previously reported for different LAs bearing either a single phenolic ring, as Lid or Ttc (Alberola-Die *et al.*, 2011; Cobo *et al.*, 2018) or two rings, as adiphenine (Spitzmaul *et al.*, 2009). In all these cases, it has been proposed to be mediated by enhancement of nAChR desensitization.

The effect of Bzc on $I_{ACh}$ decay was assessed by co-applying either 10 or 100 µM ACh with 500 µM Bzc (i.e. close to its $IC_{50}$) both at negative and positive potentials (Fig. 7). $I_{ACh}$s declined slower at 10 µM ACh (Fig. $7A_1$, $A_2$) than at 100 µM ACh (Fig. $7A_3$, $A_4$), because nAChR desensitization is dependent on ACh concentration. Interestingly, Bzc accelerated differentially the $I_{ACh}$ decays at these two ACh concentrations. Thus, at the same Bzc dose, the $I_{ACh}$ decay was significantly more accelerated when using the higher ACh concentration, both at -60 and at +40 mV (Fig. 7). This Bzc effect is better shown when plotting the $I_{ACh}$ values at different times after $I_p$ for currents elicited by 10 or 100 µM ACh either alone or co-applied with 500 µM Bzc at -60 and +40 mV (Fig. $7B_1$, $B_2$, respectively). This sharper acceleration of $I_{ACh}$ decay when Bzc was co-applied with 100 µM ACh strongly suggests that this effect is due to enhancement of nAChR desensitization instead of a slow nAChR blockade by Bzc.

Further evidences pointing out that Bzc boosts nAChR desensitization arise when plotting the ratios of $I_{ss}$ versus $I_p$ amplitudes elicited by co-applying 10 µM ACh alone or with different Bzc concentrations, which denotes the extent of desensitization (Sobolevsky *et al.*, 1999; see equation 3). As shown in Fig. 8, below 300 µM Bzc, the quotient $I_{ss}$ to $I_p$ in the presence of Bzc ($I_{ss\_Bzc}/I_{p\_Bzc}$) versus the $I_{ss}$ to $I_p$ ratio in the presence of ACh alone ($I_{ss\_Ctr}/I_{p\_Ctr}$) is close to 1. In contrast, above 300 µM Bzc, these quotients are significantly smaller than 1 ($p < 0.05$; one sample *t*-test). Furthermore, the higher $I_{ss}$ inhibition the lower is this quotient (Fig. 8A). Therefore, this plot indicates that, up to 300 µM Bzc, there is nAChR blockade without changing $I_{ACh}$ decay whereas, above 300 µM, Bzc elicits both nAChR blockade and enhancement of nAChR desensitization.

Desensitized nAChRs are characterized by a non-conductive pore while the agonist is still bound, because its affinity for the ligand is markedly increased (reviewed in

Giniatullin *et al.*, 2005; Keramidas and Lynch, 2013). Thus, to verify that Bzc, at its $IC_{50}$, is actually enhancing nAChR desensitization, we plotted the dose-response curves for $I_p$ and $I_{ss}$ in the presence and absence of Bzc, as a gauge of nAChR desensitization (Gielen and Corringer, 2018). Since, as previously mentioned, very high concentrations of ACh (above 100 µM) elicit open-channel blockade of nAChRs, $I_{ACh}$s elicited by 1 mM ACh were quite often smaller than those evoked by 100 µM ACh. Therefore, we restricted the maximum ACh concentration for these plots to 100 µM ACh. As shown in Fig. 8B, the apparent affinity ($EC_{50}$) of nAChR for ACh was slightly higher for $I_{ss}$ than for $I_p$ when $I_{ACh}$s were elicited by just ACh (CIs for the apparent $EC_{50}$s were 10.6 - 13.2 µM versus 13.0 - 29.1 µM for $I_{ss}$ and $I_p$, respectively). When $I_{ACh}$s were elicited in the presence of Bzc, the dose-response curves were shifted to the left, being particularly pronounced for $I_{ss}$ (CIs for the apparent $EC_{50}$s were 5.1 - 6.3 µM versus 11.9 - 22.7 µM for $I_{ss}$ and $I_p$, respectively). This indicates a significant increase in the apparent affinity of nAChR for ACh in the presence of Bzc and, consequently, a higher desensitization.

**Virtual docking assays**

Bzc and nAChR interactions were studied by using as template new structural models of nAChRs in the open and closed states, modifying previous Unwin's models (see Experimental Procedures section). Essentially, the new models correct some inaccuracies in the loops connecting M1-M2 helices in both the closed and the open states of *Torpedo* nAChRs. A total of 800 runs were accomplished for each conformation. The best solutions combining binding energy and frequency corresponded to 102 clusters sites differing less than 5 Å of RMSD for the nAChR in the open state and 113 clusters for the closed state. Figure 9 shows that most of these clusters were located at the ECD (55 and 58% for open and closed states, respectively) and the remaining were sited at the TMD. In both conformations, nAChR-Bzc interactions at the ECD mainly involved 2 subunits (59 and 55% for open and closed states, respectively), chiefly $\alpha_\gamma$-γ (sites 1 and 6 of Fig. 9, for open and closed nAChRs, respectively) and $\alpha_\delta$-δ, (sites 4 and 3 for open and closed states, respectively), close to the orthosteric binding site, although some clusters were intrasubunit, involving mainly the α subunits. TMD clusters were located at intra- or inter-subunit crevices, involving 1 or 2 subunits, respectively, with a clear preference for the δ subunit in both states. Thus, 17% of the total solutions in the open state were located at the β-δ inter-subunit (Fig. 9, site 7), whereas the same percentage of solutions were at a δ intra-subunit site in the

closed state (Fig. 9, site 9). Other energetically favorable sites for both states involved both α subunits. Though our binding assays did not find any Bzc cluster inside the channel pore, there were a few solutions with intersubunit binding sites near to the inner wall of the pore in the open state. Noticeably, we have found very few solutions of Bzc interactions at the M1-M2 loop or at residues close by the M2 helix in these corrected models of nAChRs and, furthermore, they showed low binding energies.

## DISCUSSION

This work is aimed to understand the mechanisms underlying the effects of Bzc on nAChRs by using two powerful experimental approaches developed by Ricardo Miledi and his group. First, the use of *Xenopus* oocytes as convenient cells to carry on detailed functional studies on nAChRs, and other ion channels, from fresh or frozen tissues of different species, including humans (Barnard *et al.*, 1982; Miledi *et al.*, 1989). Second, the microtransplantation of fully mature proteins, with their native stoichiometry, to oocytes by injecting into these cells either plasma membranes or purified and reconstituted proteins (Marsal *et al.*, 1995; Morales *et al.*, 1995; Eusebi *et al.*, 2009).

The present results confirm that Bzc inhibits muscle-type nAChRs and deepen the knowledge on the modulating mechanisms of LAs on nAChRs. Bzc and other LAs bearing a single aromatic ring, as Lid, procaine or Ttc (Group I of LAs; Arias, 1999), share certain effects on nAChRs, though there are also significant differences among them. Thus, Bzc potency as nAChR blocker ($IC_{50}$s of 220 and 382 μM for $I_{ss}$ and $I_p$, respectively) is lower than those found for Lid (11 - 73 μM; Gentry and Lukas, 2001; Wang *et al.*, 2010; Alberola-Die *et al.*, 2011) or procaine (25 - 230 μM; Adams, 1977; Koblin and Lester, 1979; Gentry and Lukas, 2001; Wang *et al.*, 2010) and much lower than that of Ttc ($IC_{50}$ in the submicromolar range; Cobo *et al.*, 2018). Besides, nAChR blockade by Bzc is voltage independent (Koblin and Lester, 1979; Odgen et al, 1981; present data), in contrast to the nAChR blockade by Lid (Alberola-Die *et al.*, 2011), procaine (Adams, 1977) or Ttc (Cobo *et al.*, 2018). Nevertheless, Bzc elicits flickering of single-channel currents from endplate nAChRs, strongly suggesting that it blocks this receptor by acting inside the pore (Odgen *et al.*, 1981). In agreement with this, the joint withdrawal of ACh and Bzc elicited $I_{Rb}$s, which might be due to relief from the Bzc open-channel blockade, in spite that our docking assays did not show Bzc binding inside the channel pore, but near to the inner wall of the pore in the open state. These

$I_{Rb}$s were more pronounced when co-applying Bzc, at roughly its $IC_{50}$, with high ACh concentrations (100 µM or 1 mM; see Fig. $4A_2$, $A_3$), though $I_{Rb}$s could be also evoked at lower ACh concentrations (10 µM) when increasing Bzc to 1 mM (Fig. 1A). Notably, the $I_{Rb}$ was voltage independent, since it was evoked when rinsing ACh and Bzc either at -60 or at +40 mV (Fig. $5A_1$, $A_2$). It has been previously reported that $I_{Rb}$s are elicited when molecules acting as open-channel blockers are withdrawn from the pore while some ACh molecules are still bound to the orthosteric site (Legendre *et al.*, 2000; Liu *et al.*, 2008; Alberola-Die *et al.*, 2016b). Although, the presence of $I_{Rb}$ points out that Bzc is acting as a conventional open-channel blocker, just plugging the pore, an additional mechanism must be considered because it was also found, though smaller, when just ACh was rinsed (Fig. $5A_1$, $A_2$). Since ACh is positively charged, its contribution to the $I_{Rb}$ by an open-channel blockade can be ruled out, because $I_{Rb}$ was still found when holding the membrane potential at +40 mV. The small $I_{Rb}$s evoked by rinsing just ACh should be triggered by the decrease of ACh concentration, which would allow some nAChRs to recover from desensitization. As desensitized nAChRs retain ACh molecules bound to the orthosteric sites with high affinity, they might gate the channel as the nAChRs leave the desensitized state, giving rise to the $I_{Rb.}$ Thus, the enhancement of nAChR desensitization by Bzc, both at negative and positive potentials (Fig. 7), would favor the rise of $I_{Rb}$ when ACh is withdrawn. Furthermore, since higher ACh concentration results in larger and faster nAChR desensitization, it would be expected that, for the same Bzc concentration, $I_{Rb}$ would increase with ACh concentration, as it actually occurs. Therefore, $I_{Rb}$ could arise from two non-exclusive mechanisms which, most likely, act combined: *i)* open-channel blockade of nAChRs by Bzc and *ii)* nAChR recovery from desensitization, which it is enhanced by Bzc and takes place at both negative and positive potentials.

Besides acting as an open-channel blocker, Bzc interacts with resting (closed) nAChRs, as evidenced by the $I_{ACh}$ inhibition elicited when Bzc was solely pre-applied (Fig. 4). This nAChR inhibition differs from that elicited by plugging the channel pore and it is characterized by a slow $I_{ACh}$ activation (Fig. 4). Noticeably, Bzc pre-application, either alone or followed by ACh and Bzc co-application, slowed down the rate of nAChR activation and, consequently the apparent time-to-peak increased (Table 1). In contrast, just ACh and Bzc co-application decreased the time-to-peak, most likely because of its open-channel blockade and enhancement of desensitization, as reported for BW284c5

(Olivera-Bravo *et al.*, 2005). Though we have no direct evidences on the mechanisms involved in the slowing down of $I_{ACh}$ activation, the virtual docking assays indicates that Bzc binds close to the orthosteric binding site on resting nAChRs, which might underlie its slow activation. Another characteristic effect of Bzc pre-applications is their long lasting inhibition of $I_{ACh}$, which surpassed the subsequent 32 s pulse of ACh (Fig. 4). Likewise, a very slow recovery of $I_{ACh}$ was also found when resting nAChRs were blocked by either Ttc (Cobo *et al.*, 2018) or DMA (A.M. unpublished results).

Furthermore, Bzc enhanced $I_{ACh}$ decay when co-applied with ACh at concentrations close to or above its $IC_{50}$ (Figs. 7, 8), as reported for Lid (Alberola-Die *et al.*, 2011) and Ttc (Cobo *et al.*, 2018). In the case of Ttc, the enhancement of nAChR desensitization seems due to its binding to M2 residues located inside the channel pore, close by the ECD-TMD interphase (Cobo *et al.*, 2018). However, in our docking assays neither Bzc nor DMA did show a high affinity for those residues (Fig. 10), in spite that $I_{ACh}$ decay acceleration by these molecules was mostly found when the channel was already gated by ACh. The process of nAChR desensitization is yet poorly understood, though it is known that not only residues within the channel pore affect the rate of desensitization, since different residues at both the ECD (Yakel, 2010) and the ICD (Giniatullin, 2005; Shen, 2005) have been also involved.

As previously mentioned, Lid actions on nAChRs (Alberola-Die *et al.*, 2011) have been dissected by using analogues of both its hydrophilic (DEA) and hydrophobic (DMA) moieties. Thus, some Lid actions on this receptor overlapped with those of DEA, whereas others matched fairly well those elicited by DMA (Alberola-Die *et al.*, 2016a, b). Remarkably, DEA and Ttc are molecules largely protonated at pH 7, but they differ widely in their actions on nAChRs. For instance, in contrast to DEA, Ttc markedly enhances nAChR desensitization, and the putative binding sites of Ttc and DEA on nAChRs, as deduced from virtual docking assays, are fairly different (Alberola-Die *et al.*, 2016a; Cobo *et al.*, 2018). However, most of the Bzc effects on nAChRs reported above remind those elicited by DMA. Thus, Bzc and DMA share, at least, the following effects on nAChRs: *i)* low blocking potency, with $IC_{50}$s close to 1 mM; *ii)* voltage-independent blockade, though they seem to bind inside the channel pore, eliciting open-channel blockade; *iii)* pharmacological profile corresponding to non-competitive blockade; *iv)* marked $I_{Rb}$s during the washout phase, both at negative and positive potentials; *iv)* blockade of resting nAChRs, unraveled by Bzc application before

challenging the cell with ACh (pre-application protocol); *v)* slowed down $I_{ACh}$ activation in pre-application protocols, particularly when testing high ACh concentrations; *vi)* enhancement of nAChR desensitization; *vii)* binding sites on the nAChR mainly located at the ECD (close to the orthosteric binding site and at the δ subunit) and at the TMD (particularly at intra- and inter-subunit crevices in the δ subunit, both in the open and closed states); and *viii*) blockade of $GABA_A$Rs, decreasing the peak-current amplitude, accelerating the $I_{GABA}$ decay and eliciting $I_{Rb}$s. Consequently, since DMA effects on muscle-type nAChRs mimic fairly well those elicited by the unprotonated form of Lid, it follows that Bzc and uncharged Lid molecules overlap their mechanisms of action on nAChRs. Moreover, these mechanisms largely differ from those reported for charged LAs, as Ttc (Cobo *et al.*, 2018) or other related molecules, as DEA (Alberola-Die *et al.*, 2016a).

In conclusion, this work demonstrates that $I_{ACh}$ blockade by Bzc involves different mechanisms of nAChR inhibition, which are summarized in Figure 11. These results contribute to better understanding either how certain therapeutic molecules, as LAs, affect nAChR function and point out the putative binding sites for these molecules at the nAChR. These results shed new light on how these molecules elicit some of their clinical side effects and even might help in the design of new therapeutic molecules acting on this subfamily of LGICs. This is of a great relevance because nAChRs are involved in multiple pathological processes, including neurodegenerative diseases, nicotine addiction, schizophrenia, certain types of epilepsy, congenital myasthenia, inflammation or pain (Hurst *et al.*, 2013; Wu *et al.*, 2015; Parikh *et al.*, 2016; Schulte *et al.*, 2016).

REFERENCES

Adams, P. R. (1977). Voltage jump analysis of procaine action at frog end-plate. *J. Physiol*. 268, 291-318. doi: 10.1113/jphysiol.1977.sp011858.

Alberola-Die, A., Fernández-Ballester, G., González-Ros, J. M., Ivorra, I., and Morales, A. (2016a). Muscle-Type Nicotinic Receptor Blockade by Diethylamine, the Hydrophilic Moiety of Lidocaine. *Front. Mol. Neurosci*. 9:12. doi: 10.3389/fnmol.2016.00012.

Alberola-Die, A., Fernández-Ballester, G., González-Ros, J. M., Ivorra, I., and Morales, A. (2016b). Muscle-type nicotinic receptor modulation by 2,6-dimethylaniline, a molecule resembling the hydrophobic moiety of lidocaine. *Front. Mol. Neurosci*. 9:127. doi: 10.3389/fnmol.2016.00127.

Alberola-Die, A., Reboreda, A., Lamas, J. A., and Morales, A. (2013). Lidocaine effects on acetylcholine-elicited currents from mouse superior cervical ganglion neurons. *Neurosci. Res*. 75, 198-203. doi: 10.1016/j.neures.2013.01.005.

Alberola-Die A., Martínez-Pinna J., González-Ros J.M., Ivorra I. and Morales A. (2011). Multiple inhibitory actions of lidocaine on *Torpedo* nicotinic acetylcholine receptors transplanted to *Xenopus* oocytes. *J. Neurochem*. 117, 1009-1019. doi: 10.1111/j.1471-4159.2011.07271.x.

Albuquerque, E. X., Pereira, E. F. R., Alkondon, M., and Rogers, S. W. (2009). Mammalian acetylcholine receptors: from structure to function. *Physiol. Rev*. 89, 73-120. doi: 10.1152/physrev.00015.2008.

Arias, H. R. (1999). Role of local anesthetics on both cholinergic and serotonergic ionotropic receptors. *Neurosci. Biobehav. Rev*. 23, 817-843. doi: 10.1016/S0149-7634(99)00020-2.

Barnard, E. A., Miledi, R., and Sumikawa, K. (1982). Translation of exogenous messenger RNA coding for nicotinic acetylcholine receptors produces functional receptors in *Xenopus* oocytes. *Proc. R. Soc. Ser. B-Bio*. 215, 241-246. doi: 10.1098/rspb.1982.0040.

Bouzat, C., and Mukhtasimova, N. (2018). The nicotinic acetylcholine receptor as a molecular machine for neuromuscular transmission. *Current Opinion in Physiology*. 4, 40-48. doi: https://doi.org/10.1016/j.cophys.2018.04.008.

Catterall, W.A. and Mackie, K. (2001). Local anesthetics. In: Goodman and Gilman's the pharmacological basis of therapeutics. (Hardman, J.G., Limbird, L.E., Molinoff, P.B., Ruddon, R.W., Gilman, A.G., eds.), pp. 367-84. New York: Macmillan.

Cobo, R., Nikolaeva, M., Alberola-Die, A., Fernandez-Ballester, G., González-Ros, J. M., Ivorra, I., and Morales, A. (2018). Mechanisms underlying the strong inhibition of muscle-type nicotinic receptors by tetracaine. *Front. Mol. Neurosci*. 11: 193. doi: 10.3389/fnmol.2018.00193.

Cobo, R., Alberola-Die, A., Ivorra, I., Morales A. (2016) *J. Physiol. Biochem.* 72 (Suppl. 1): S43.

Deguchi, T., Narahashi, T. (1971). Effects of procaine on ionic conductances of end-plate membranes. *J. Pharmacol. Exp. Ther*. 176, 423-433.

Di Croce, D., Trinks, P. W., Grifo, M. B., Takara, D., and Sánchez, G. A. (2015). Drug action of benzocaine on the sarcoplasmic reticulum Ca-ATPase from fast-twitch skeletal muscle. *N-S Arch. Pharmacol*. 388, 1163–1170. doi: 10.1007/s00210-015-1149-7.

Duan, Y., Wu, C., Chowdhury, S., Lee, M. C., Xiong, G., Zhang, W., *et al.* (2003). A point-charge force field for molecular mechanics simulations of proteins based on condensed-phase quantum mechanical calculations. *J. Comput. Chem*. 24, 1999-2012. doi: 10.1002/jcc.10349.

Eusebi, F., Palma, E., Amici, M., and Miledi, R. (2009). Microtransplantation of ligand-gated receptor-channels from fresh or frozen nervous tissue into *Xenopus* oocytes: A potent tool for expanding functional information. *Prog. Neurobiol*. 88, 32-40. doi: 10.1016/j.pneurobio.2009.01.008.

Fukuda, K., Nakajima, T., Viswanathan, P. C., and Balser, J. R. (2005). Compound-specific $Na^+$ channel pore conformational changes induced by local anaesthetics. *J. Physiol*. 564, 21-31. doi: 10.1113/jphysiol.2004.081646.

Gentry, C. L., and Lukas, R. J. (2001). Local anesthetics noncompetitively inhibit function of four distinct nicotinic acetylcholine receptor subtypes. *J. Pharmacol. Exp. Ther*. 299, 1038–1048.

Gielen, M., and Corringer, P.-J. (2018). The dual-gate model for pentameric ligand-gated ion channels activation and desensitization. *J. Physiol*. 596, 1873-1902. doi: 10.1113/JP275100.

Giniatullin, R., Nistri, A., and Yakel, J. L. (2005). Desensitization of nicotinic ACh receptors: Shaping cholinergic signaling. *Trends Neurosci.* 28, 371-378. doi: 10.1016/j.tins.2005.04.009.

Guex, N., and Peitsch, M. C. (1997). SWISS-MODEL and the Swiss-PdbViewer: an environment for comparative protein modeling. *Electrophoresis* 18, 2714–2723. doi: 10.1002/elps.1150181505.

González-Rodríguez, A. J., Gutiérrez-Paredes, E. M., Revert Fernández, A., and Jordá-Cuevas, E. (2013). Allergic contact dermatitis to Benzocaine: The importance of concomitant positive patch test results. *Actas Dermosifiliogr*. 104, 156-158. doi: 10.1016/j.ad.2011.07.023

Hille, B. (1966). Common mode of action of three agents that decrease the transient change in sodium permeability in nerves. *Nature* 210, 1220-1222.

Hurst, R., Rollema, H., and Bertrand, D. (2013). Nicotinic acetylcholine receptors: from basic science to therapeutics. *Pharmacol. Therapeut*. 137, 22-54. doi: 10.1016/j.pharmthera.2012.08.012

Ivorra I., Fernández A., Gal B., Aleu J., González-Ros J. M., Ferragut J. A., *et al.* (2002). Protein orientation affects the efficiency of functional protein transplantation into the *Xenopus* oocyte membrane. *J. Membr. Biol*. 185, 117–127. 10.1007/s00232-001-0118-x

Katz, B., and Miledi, R. (1975). The effect of procaine on the action of acetylcholine at the neuromuscular junction. *J. Physiol.* 249, 269-284. doi: 10.1113/jphysiol.1975.sp011015.

Keramidas, A., and Lynch, J. W. (2013). An outline of desensitization in pentameric ligand-gated ion channel receptors. *Cell. Mol. Life Sci.* 70, 1241-1253. doi: 10.1007/s00018-012-1133-z.

Koblin, D. D., and Lester, H. A. (1979). Voltage-dependent and voltage-independent blockade of acetylcholine receptors by local anesthetics in *Electrophorus* electroplaques. *Mol. Pharmacol*. 15, 559-580.

Kordas, M. (1970). The effect of procaine on neuromuscular transmission. *J. Physiol*. 209, 689-699. doi: 10.1113/jphysiol.1970.sp009186.

Krieger, E., Koraimann, G., and Vriend, G. (2002). Increasing the precision of comparative models with YASARA NOVA; a self-parameterizing force field. *Proteins* 47, 393–402. doi: 10.1002/prot.10104.

Kusano, K., Miledi, R., and Stinnakre, J. (1982). Cholinergic and catecholaminergic receptors in the *Xenopus* oocyte membrane. *J. Physiol*. 328, 143–170. doi: 10.1113/jphysiol.1982.sp014257.

Laskowski, R. A., Rullmannn, J. A., MacArthur, M. W., Kaptein, R. and Thornton, J. M. (1996). AQUA and PROCHECK-NMR: programs for checking the quality of protein structures solved by *NMR. J. Biomol. NMR.* 8, 477-486. doi: 10.1007/BF00228148.

Legendre, P., Ali, D. W., and Drapeau, P. (2000). Recovery from open channel block by acetylcholine during neuromuscular transmission in zebrafish. *J. Neurosci*. 20, 140-8. doi: 10.1523/JNEUROSCI.20-01-00140.2000.

Liu Q., Yu K., Chang Y., Lukas R. J., and Wu J. (2008). Agonist-induced hump current production in heterologously –expressed human α4β2-nicotinic acetylcholine receptors. *Acta Pharmacol. Sin*. 29, 305-319. doi: 10.1111/j.1745-7254.2008.00760.x.

Mantipragada, S.B., Horváth, L. I., Arias, H. R., Schwarzmann, G., Sandhoff, K., Barrantes, F. J., and Marsh, D. (2003). Lipid−protein interactions and effect of Local anesthetics in acetylcholine receptor-rich membranes from *Torpedo marmorata* electric organ. *Biochemistry.* 42, 9167-9175. doi: 10.1021/bi034485q

Marsal, J., Tigyi, G., and Miledi, R. (1995). Incorporation of acetylcholine receptors and $Cl^-$ channels in *Xenopus* oocytes injected with *Torpedo* electroplaque membranes. *Proc. Natl. Acad. Sci. U.S.A.* 92, 5224-5228. doi: 10.1073/pnas.92.11.5224.

Middleton, R. E., Strnad, N. P., and Cohen, J. B. (1999). Photoaffinity labeling the *Torpedo* nicotinic acetylcholine receptor with [3H]tetracaine, a nondesensitizing noncompetitive antagonist. *Mol. Pharmacol*. 56, 290–299. doi: 10.1124/mol.56.2.290.

Miledi, R., Parker, I., and Sumikawa, K. (1989) Transplanting receptors from brains into oocytes. In: *Fidia Research Foundation Neuroscience Award Lectures* 3. Raven Press, New York, pp. 57–90.

Morales, A., Aleu, J., Ivorra, I., Ferragut, J. A., González-Ros, J. M., and Miledi, R. (1995). Incorporation of reconstituted acetylcholine receptors from *Torpedo* into the *Xenopus* oocyte membrane. *Proc. Natl. Acad. Sci. U.S.A.* 92, 8468–8472. doi: 10.1073/pnas.92.18.8468.

Morris, G. M., Huey, R., and Olson, A. J. (2008). Using AutoDock for ligand receptor docking. *Curr. Protoc. Bioinformatics,* Chapter 8: Unit 8.14. doi: 10.1002/0471250953.bi0814s24

Neher, E., and Steinbach, J. H. (1978). Local anaesthetics transiently block currents through single acetylcholine-receptor channels. *J. Physiol*. 277, 153-176. doi: 10.1113/jphysiol.1978.sp012267.

Newcombe, J., Chatzidaki, A., Sheppard, T. D., Topf, M., and Millar, N. (2018). Nicotinic acetylcholine receptor positive allosteric modulators revealed by mutagenesis and a revised structural model. *Mol. Pharmacol.* 93, 128-140. doi: https://doi.org/10.1124/mol.117.110551.

Ogden, D. C., Siegelbaum, S. A., and Colquhoun, D. (1981). Block of acetylcholine-activated ion channels by an uncharged local anaesthetic. *Nature*. 289, 596-598.

Olivera-Bravo, S., Ivorra, I., and Morales, A. (2007). Diverse inhibitory actions of quaternary ammonium cholinesterase inhibitors on *Torpedo* nicotinic ACh receptors transplanted to *Xenopus* oocytes. *Br. J. Pharmacol*. 151, 1280-1292. doi: 10.1038/sj.bjp.0707329.

Olivera-Bravo S., Ivorra I., and Morales A. (2005). The acetylcholinesterase inhibitor BW284c51 is a potent blocker of *Torpedo* nicotinic AchRs incorporated into the *Xenopus* oocyte membrane. *Br. J. Pharmacol*. 144, 88-97. doi: 10.1038/sj.bjp.0705965.

Pascual, J. M., and Karlin, A. (1998). Delimiting the binding site for quaternary ammonium lidocaine derivatives in the acetylcholine receptor channel. *J. Gen. Physiol*. 112, 611–621. Doi: 10.1085/jgp.112.5.611.

Parikh, V., Kutlu, M. G., and Gould, T. J. (2016). nAChR dysfunction as a common substrate for schizophrenia and comorbid nicotine addiction: current trends and perspectives. *Schizophr. Res*. 171, 1–15. doi: 10.1016/j.schres.2016.01.020.

Schulte, M. K., Khatri, S., Huang, Y., DeCristofano, L., and LeBlanc, G. G. (2016). Allosteric modulation and potential therapeutic applications of heteromeric nicotinic acetylcholine receptors. *Neurotransmitter* 3, e1275. doi: 10.14800/nt.1275.

Schwede, T., Kopp, J., Guex, N. and Peitsch, M. C. (2003). SWISS-MODEL: An automated protein homology-modeling server. *Nucleic Acids Res*. 31, 3381-3385. doi: 10.1093/nar/gkg520.

Shen, X.-M., Ohno, K., Sine, S. M., and Engel, A. G. (2004). Subunit-specific contribution to agonist binding and channel gating revealed by inherited mutation in muscle acetylcholine receptor M3-M4 linker. *Brain*. 128, 345–355. doi: 10.1093/brain/awh364.

Sievers, F., Wilm, A. O., Dineen, D., Gibson, T.J.O., Karplus, K., Li, W.O., Lopez, R.O., McWilliam, H.O. *et al.* (2011). Fast, scalable generation of high-quality protein multiple sequence alignments using Clustal Omega. *Molecular Systems Biology* 7:539. doi: 10.1038/msb.2011.75.

Sine, S. M. (2012). End-Plate acetylcholine receptor: Structure, mechanism, pharmacology, and disease. *Physiol. Rev*. 92, 1189–1234. doi: 10.1152/physrev.00015.2011.

Sine, S. M., & Steinbach, J. H. (1984). Activation of a nicotinic acetylcholine receptor. Biophys. J. 45, 175–185. doi: 10.1016/S0006-3495(84)84146-6.

Sobolevsky, A. I., Koshelev, S. G., and Khodorov, B. I. (1999). Probing of NMDA channels with fast blockers. *J. Neurosci*. 19, 10611–10626. doi: 10.1523/JNEUROSCI.19-24-10611.1999

Spitzmaul, G., Gumilar, F., Dilger, J. P., and Bouzat, C. (2009). The local anaesthetics proadifen andadiphenine inhibit nicotinic receptors by different molecular mechanisms. *Br. J. Pharmacol*. 157, 804–817. doi: 10.1111/j.1476-5381.2009.00214.x

Steinbach, A. B. (1968). Alteration by xylocaine (lidocaine) and its derivatives of the time course of the end-plate potential. *J. Gen. Physiol*. 52, 144-161.

Toyoshima, C., and Unwin, N. (1988). Contrast transfer for frozen-hydrated specimens: determination from pairs of defocused images. *Ultramicroscopy*. 25, 279-291. doi: 10.1016/0304-3991(88)90003-4.

Unwin, N. (2005). Refined structure of the nicotinic acetylcholine receptor at 4 Å resolution. *J. Mol. Biol*. 346, 967–989. doi: 10.1016/j.jmb.2004.12.031.

Unwin, N. (1995). Acetylcholine receptor channel imaged in the open sate. *Nature*. 373, 37–43. doi: 10.1038/373037a0.

Unwin, N., and Fujiyoshi, Y., (2012). Gating movement of acetylcholine receptor caught by plunge-freezing. *J. Mol. Biol.* 422, 617-634. doi: 10.1016/j.jmb.2012.07.010.

Wang, H., Zhang, Y., and Li, S. (2010). The effect of local anesthetics on the inhibition of adult muscle-type nicotinic acetylcholine receptors by nondepolarizing muscle relaxants. *Eur. J. Pharmacol.* 630, 29–33. doi: 10.1016/j.ejphar.2009.12.028.

Wu, Z. S., Cheng, H., Jiang, Y., Melcher, K., and Xu, H. E. (2015). Ion channels gated by acetylcholine and serotonin: structures, biology, and drug discovery. *Acta Pharmacol. Sin*. 36, 895–907. doi: 10.1038/aps.2015.66.

Yakel, J. L. (2010). Gating of nicotinic ACh receptors: latest insights into ligand binding and function. *J. Physiol.* 588, 597–602.

## Conflict of Interest

The authors declare that the research was conducted in the absence of any commercial or financial relationships that could be considered as a potential conflict of interest.

## Author Contributions

All signing authors have contributed substantially to the conception of this work and to the acquisition, analysis and interpretation of the data presented. Besides, all of them have participated in drafting and revising the submitted manuscript and have approved the version submitted for publication.


## Funding

This work was supported by grants BFU2012-31359, BFU2015-66612-P, SAF2015-66275-C2-1-R and SAF2017-82977-P (AEI/FEDER, UE) from MINECO, PROMETEO/2014/11 from Generalitat Valenciana (Spain) and GRE17-01 from Universidad de Alicante. R.C. held a predoctoral fellowship from Universidad de Alicante (FPUUA36) and M.N. a predoctoral industrial fellowship from Ministerio de Economía, Industria y Competitividad (DI-16-08303).

## Acknowledgments

We thank Mr. Simón Moya for expert technical assistance.

**Table 1. Effects of 500 μM Bzc on apparent time-to-$I_p$**

| *Test* | *Apparent time-to-$I_p$ (s)* | *Oocytes* | *Donors* |
|---|---|---|---|
| Control **(10 μM ACh)** | 6.5 ± 0.5 | 44 | 5-7 |
| ACh + Bzc co-app. | 2.8 ± 0.4***** | 18 | 8 |
| Bzc pre-app. | 8.1 ± 1.2 | 11 | 5 |
| Bzc pre-app. & ACh + Bzc co-app. | 5.6 ± 0.8 | 15 | 7 |
| Control **(100 μM ACh)** | 2.6 ± 0.1 | 50 | 6-7 |
| ACh + Bzc co-app. | 1.4 ± 0.2***** | 19 | 7 |
| Bzc pre-app. | 6.7 ± 0.6***** | 16 | 7 |
| Bzc pre-app. & ACh + Bzc co-app. | 6.1 ± 0.6***** | 15 | 6 |
| Control **(1000 μM ACh)** | 1.4 ± 0.1 | 18 | 2-4 |
| ACh + Bzc co-app. | 0.7 ± 0.2***** | 9 | 4 |
| Bzc pre-app. | 6.8 ± 0.5***** | 6 | 2 |
| Bzc pre-app. & ACh + Bzc co-app. | 4.1 ± 0.2***** | 3 | 2 |

(*) indicates significant differences respect to its control group.

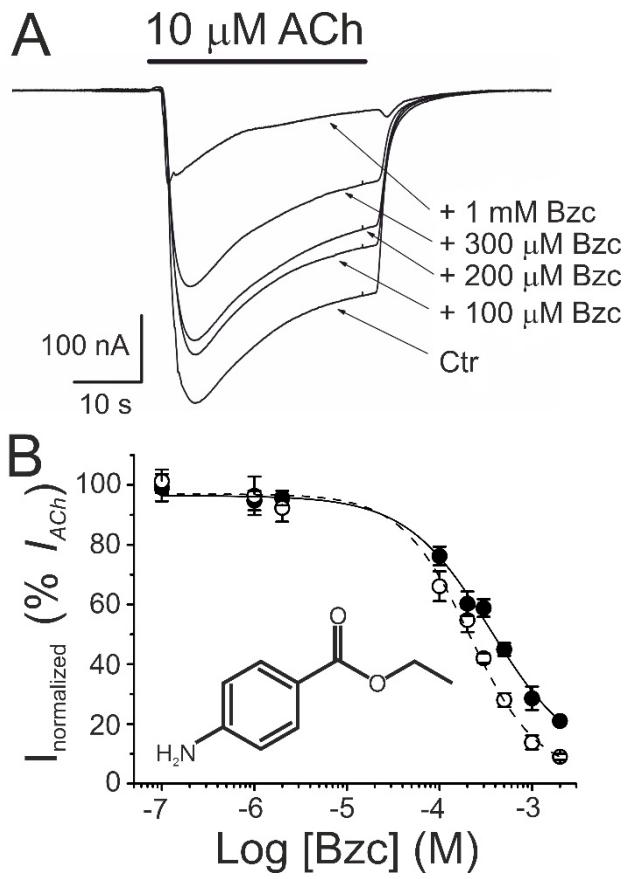


**Figure 1.** *Benzocaine (Bzc) inhibition of acetylcholine-elicited currents ($I_{ACh}$s).* **(A)** Superimposed $I_{ACh}$s evoked by 10 μM ACh either alone (Ctr) or co-applied with different Bzc concentrations, as stated on the right. Note that Bzc, at 300 μM or above, accelerates $I_{ACh}$ decay. Henceforth, unless otherwise stated, the holding potential was -60 mV, downward deflections represent inward currents and the bars above recordings indicate the timing of drug application. **(B)** Bzc concentration-$I_{ACh}$ inhibition relationship. $I_{ACh}$ amplitudes at their peak ($I_p$; filled symbols) and at their steady-state ($I_{ss}$, measured 20 s after the peak; opened symbols) elicited in the presence of Bzc were normalized to the $I_{ACh}$ evoked by ACh alone (Ctr) and plotted against the logarithm of Bzc concentration. Solid and dashed lines are sigmoid curves fitted to $I_p$ and $I_{ss}$ data, respectively. Error bars indicate SEM. Each point is the average of 3-20 oocytes from 1-10 frogs. Inset shows the molecular structure of Bzc.

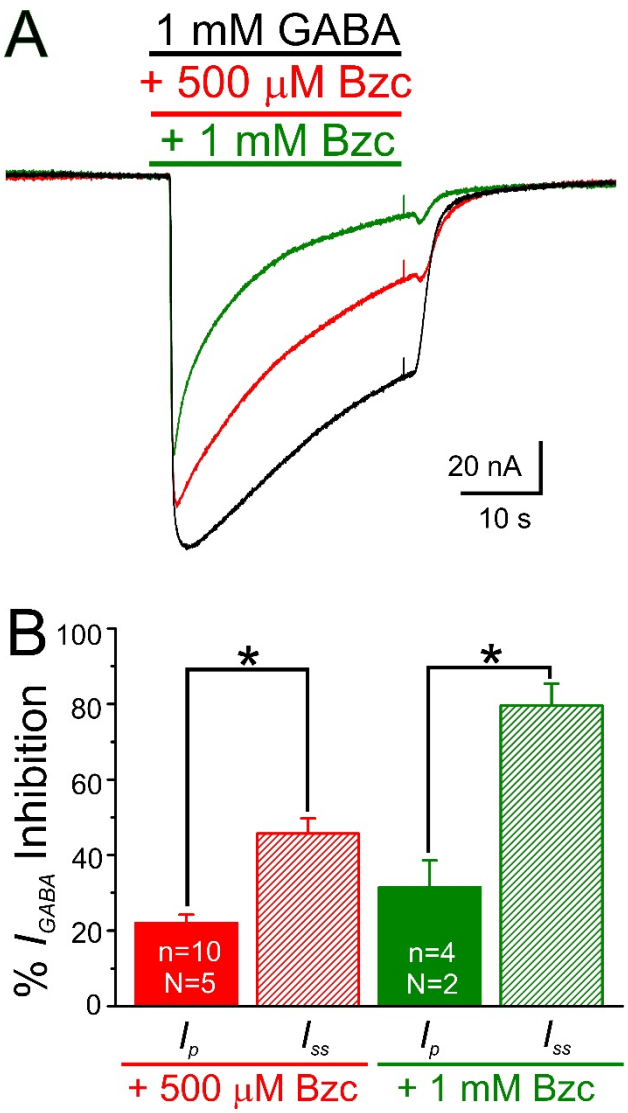


**Figure 2.** *Blockade of GABA elicited currents ($I_{GABA}$) by Bzc.* **A**. Superimposed $I_{GABA}$s elicited by 1 mM GABA alone (black recording) or together with either 500 µM (red trace) or 1 mM (green recording) Bzc in an oocyte previously injected with synaptosomal-enriched membranes. Notice that Bzc reduced the $I_{GABA}$ and sped up the $I_{GABA}$ decay in a dose-dependent way. **B**. Column graph showing the percentage of $I_{GABA}$ inhibition by 500 µM (red columns) or 1 mM (green bars) Bzc. Notice that, at both concentrations of Bzc, $I_{GABA}$ inhibition was larger at the steady-state ($I_{ss}$, striped columns) than at its peak ($I_p$, filled bars). Asterisks indicate statistically significant differences among $I_p$ and $I_{ss}$ inhibition ($p < 0.05$, paired *t*-test). The number of oocytes (n) and donor-frogs (N) is indicated in each column.

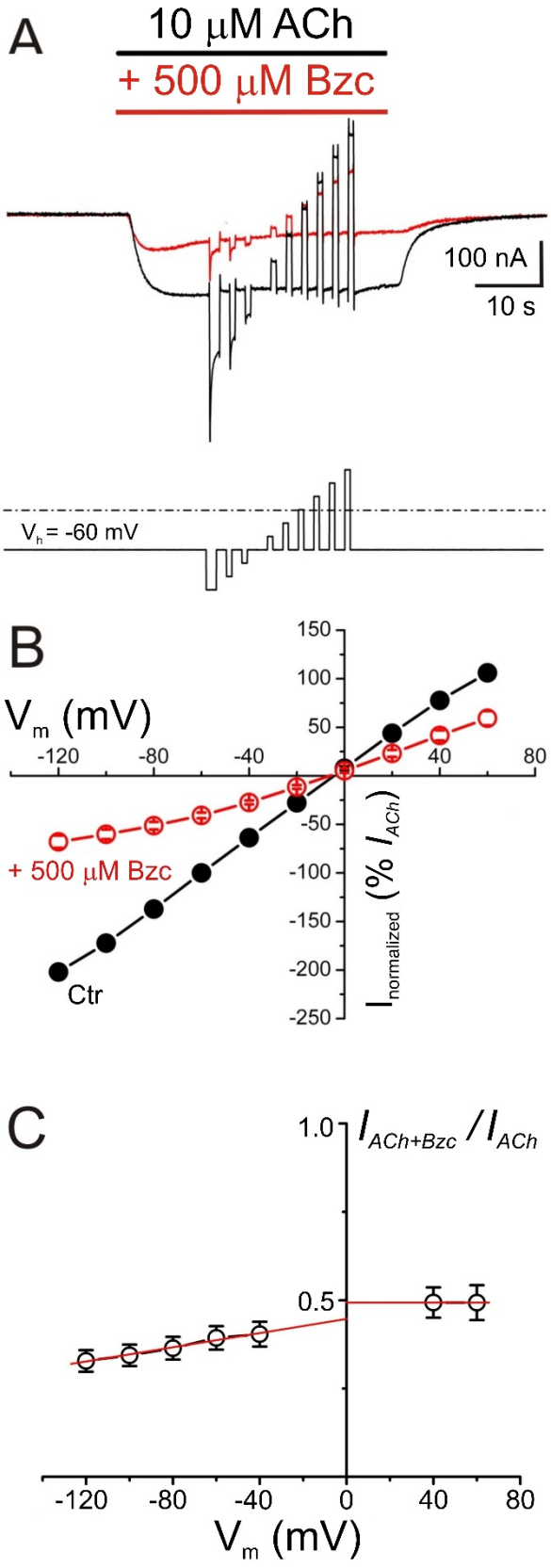


**Figure 3.** *Voltage-dependence of nAChR blockade by Bzc.* **(A)** $I_{ACh}$s evoked by 10 µM ACh alone (black recording) or in the presence of 500 µM Bzc (red recording) when the voltage pulses shown underneath were applied. **(B)** Net *i/v* relationship of $I_{ACh}$s elicited

by the protocol shown in **A**. Black symbols are for control $I_{ACh}$s (Ctr), whereas those evoked in the presence of 500 µM Bzc (+ 500 µM Bzc) are drawn in red. Net $I_{ACh}$s were normalized as their percentage of their control $I_{ACh}$ at -60 mV (n=10; N=3). (**C**) Plot showing the $I_{ACh}$s left by 500 µM Bzc ($I_{ACh+Bzc}$), normalized to their control ($I_{ACh}$), versus the membrane potential (same cells as in **B**). The lines show the best linear fit to the data at either negative or positive potentials. Despite data at negative potentials fitted fairly well to a linear function ($r^2 = 0.978$), the normalized values of remnant $I_{ACh}$ at the tested potentials showed not significant differences ($p > 0.05$, ANOVA test).

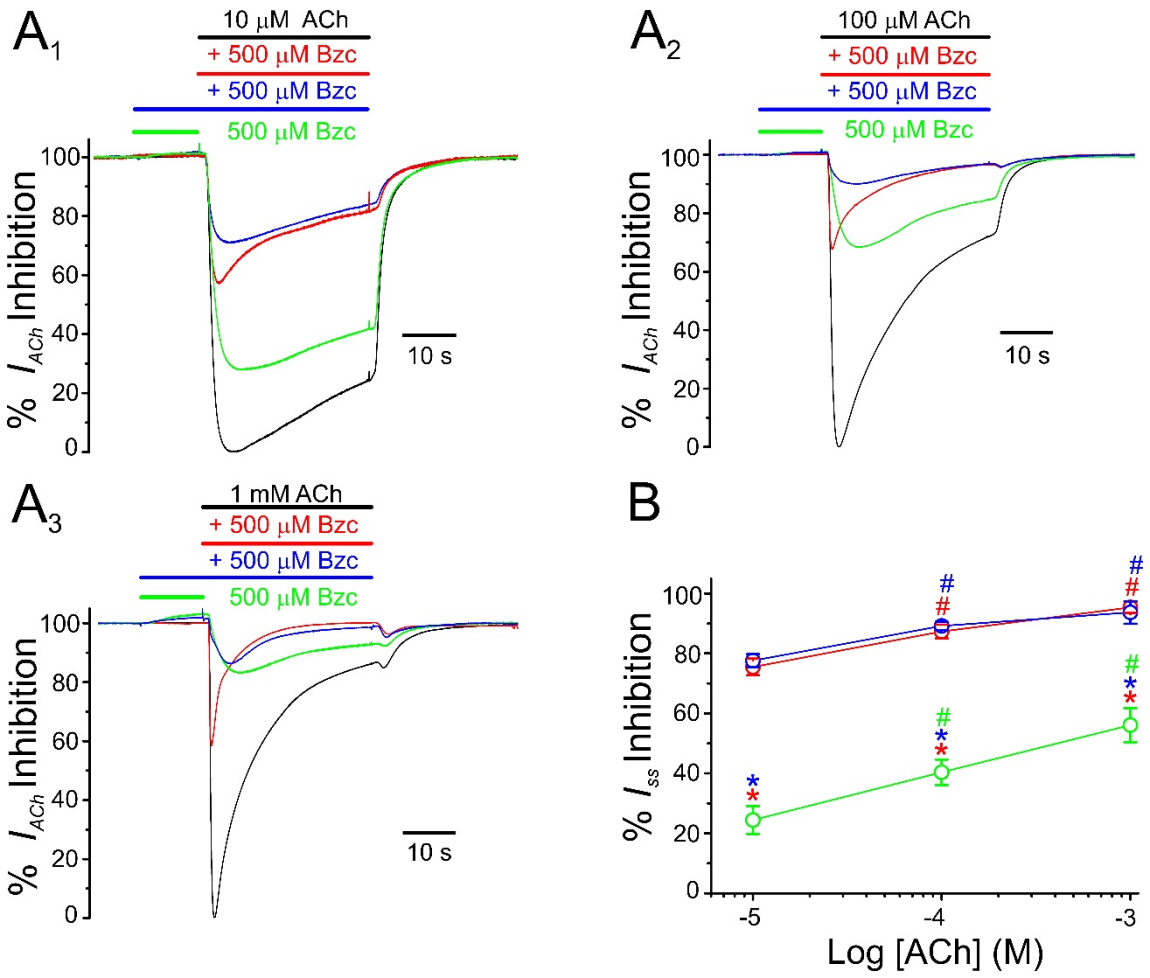


**Figure 4.** *Bzc effects on ACh concentration-$I_{ACh}$ amplitude relationship.* $I_{ACh}$*s* evoked by ACh at 10 µM (**$A_1$**), 100 µM (**$A_2$**) or 1 mM (**$A_3$**) alone (black recordings), following a pre-application of 500 µM Bzc (green recordings; **$A_1$**, **$A_2$**, **$A_3$**), when co-applied with 500 µM Bzc (red recordings; **$A_1$**, **$A_2$**, **$A_3$**), or when it was pre- and co-applied with 500 µM Bzc (blue recordings; **$A_1$**, **$A_2$**, **$A_3$**). Each trace is the average of individual recordings ("n" and "N" are those indicated in **Table 1**) previously normalized to their control $I_{ACh}$, at the indicated agonist concentrations. (**B**) Percentage of $I_{ss}$ inhibition elicited by 500 µM Bzc when tested, at different ACh concentrations, in solely pre-application (green), co-application (red) or pre- and co-application protocols (blue). Asterisks indicate significant differences in $I_{ss}$ between protocols, for each ACh concentration ($p < 0.05$, ANOVA test). Pound signs indicate significant differences among $I_{ss}$ inhibition at 10 µM ACh and other concentrations, for each experimental procedure ($p < 0.05$, ANOVA test; same cells and donors as in panels $A_1$-$A_3$).

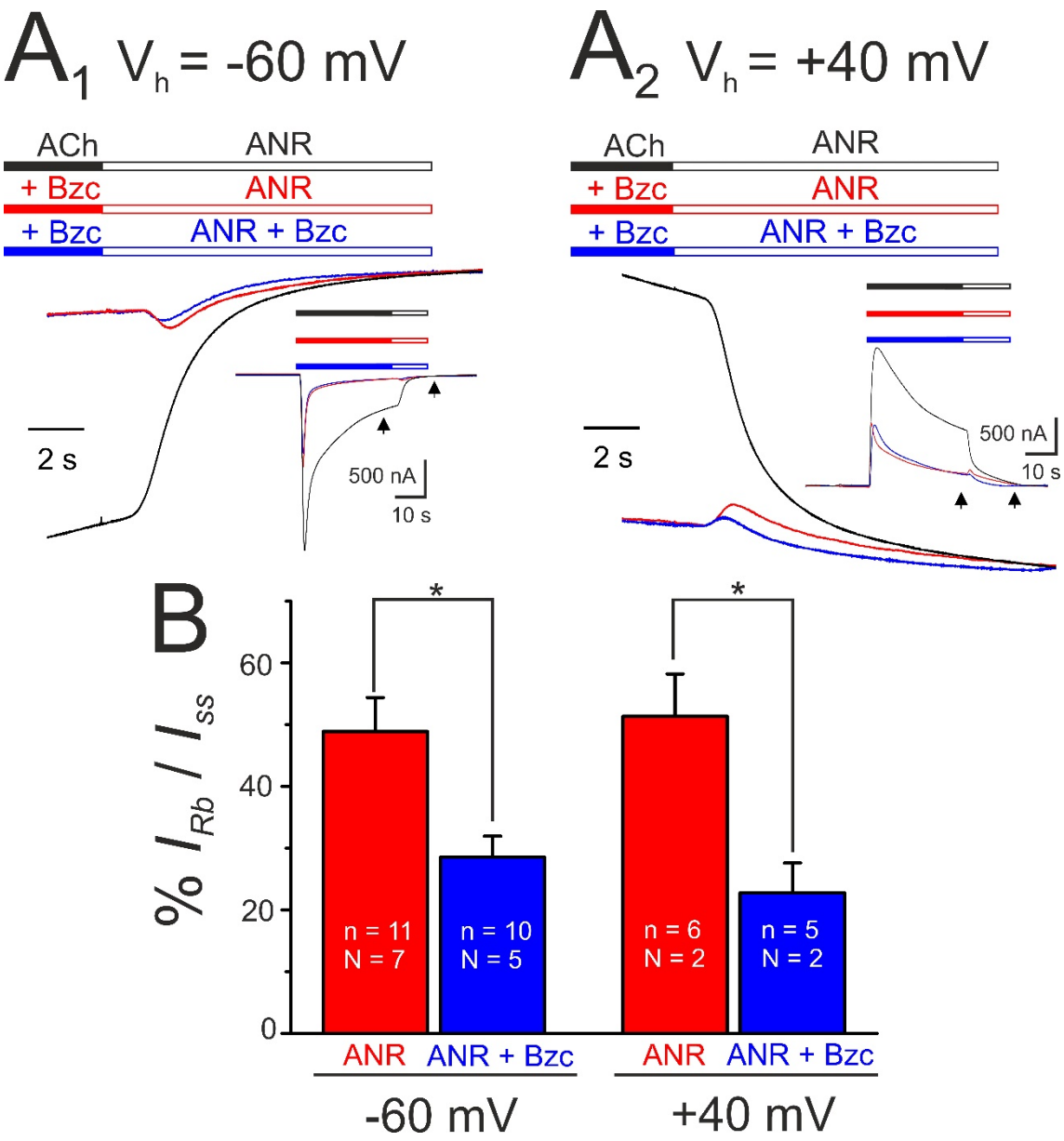


**Figure 5.** *$I_{ACh}$ rebound ($I_{Rb}$) elicited by Bzc.* (**$A_1$**, **$A_2$**) *$I_{ACh}$*s evoked by 100 µM ACh either alone (black recording and black filled bar above) or co-applied with 500 µM Bzc (red and blue recordings and filled bars) are shown as insets. The interval indicated by the arrows is shown at an expanded scale. *$I_{Rb}$*s were elicited, after co-applying ACh and Bzc, when rinsing to ANR (alone or with Bzc), as indicated by the open bars above the recordings, both at -60 (**$A_1$**) and at +40 mV (**$A_2$**). Notice the *$I_{Rb}$*s were found either when rinsing to just ANR (red recordings in **$A_1$** and **$A_2$**) or if Bzc remained in the ANR (blue recordings in **$A_1$** and **$A_2$**). In contrast, when *$I_{ACh}$*s were evoked by just ACh (black recordings, **$A_1$** and **$A_2$**), there were not *$I_{Rb}$*s. (**B**) Column graph showing normalized *$I_{Rb}$* amplitudes (see Experimental Procedures) when rinsing to ANR (red columns, 48.9 ±

5.5% versus 51.4 ± 6.8% at -60 mV and +40 mV, respectively; $p > 0.05$, *t*-test) or to ANR plus Bzc (blue columns, 28.5 ± 3.4% versus 22.8 ± 4.8% at -60 mV and +40 mV, respectively; $p > 0.05$, *t*-test). Asterisks indicate significant differences between protocols at each holding voltage ($p < 0.05$, *t*-test). Number of cells and donor-frogs are indicated in each column.

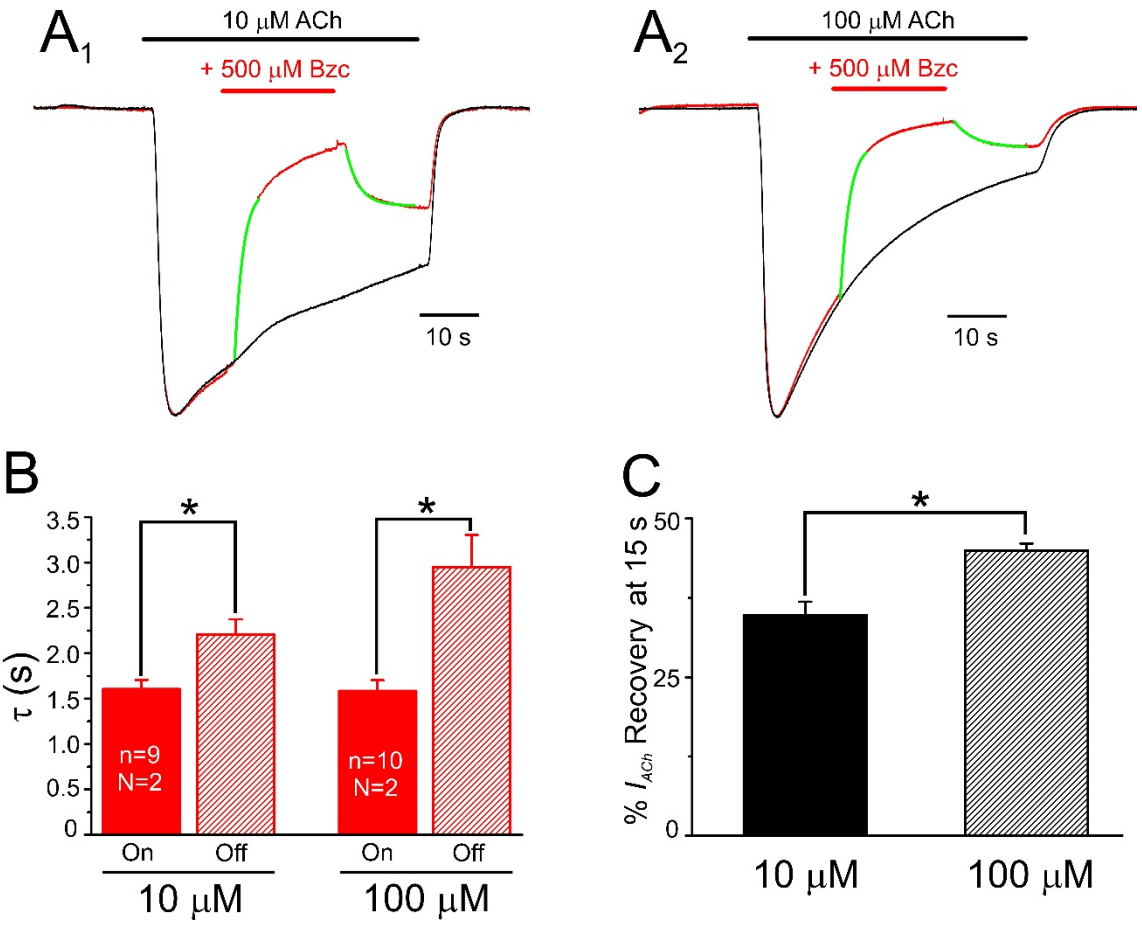


**Figure 6.** *Effects of Bzc on open-channel nAChRs.* (**A$_1$**, **A$_2$**) Superimposed $I_{ACh}$s elicited by 50 s pulses of 10 (**A$_1$**) or 100 μM ACh (**A$_2$**) either alone (black recordings) or together with 500 μM Bzc, applied at the time indicated by the red horizontal bar (red recordings in **A$_1$**, **A$_2$**). $I_p$s were normalized to the same amplitude to facilitate the kinetics comparisons. The kinetics of $I_{ACh}$ inhibition and its recovery from blockade followed exponential functions (green traces in **A$_1$**, **A$_2$**). (**B**) Column graphs showing the time constant values (τ) obtained for $I_{ACh}$ blockade onset (On, red filled columns) and for its recovery (Off, red striped columns). The rates of $I_{ACh}$ inhibition onset (1.6 ± 0.1 s, for both 10 and 100 μM ACh) were limited by the solution exchange kinetics, but those for $I_{ACh}$ recovery, after Bzc removal, were not (2.2 ± 0.2 s and 3.0 ± 0.4 s for $I_{ACh}$s elicited by 10 and 100 μM ACh, respectively). Asterisk indicates significant differences among groups ($p < 0.05$, ANOVA and Bonferroni *t*-test). (**C**) Percentage of $I_{ACh}$ recovery from blockade, 15 s after Bzc washout, for $I_{ACh}$s elicited by 10 (34.8 ± 2.1%, black filled column) or 100 μM ACh (45.0 ± 1.1%, black striped column). Asterisks indicate significant differences ($p < 0.05$, *t*-test; same number of oocytes and donor-frogs than in panel **B)**.

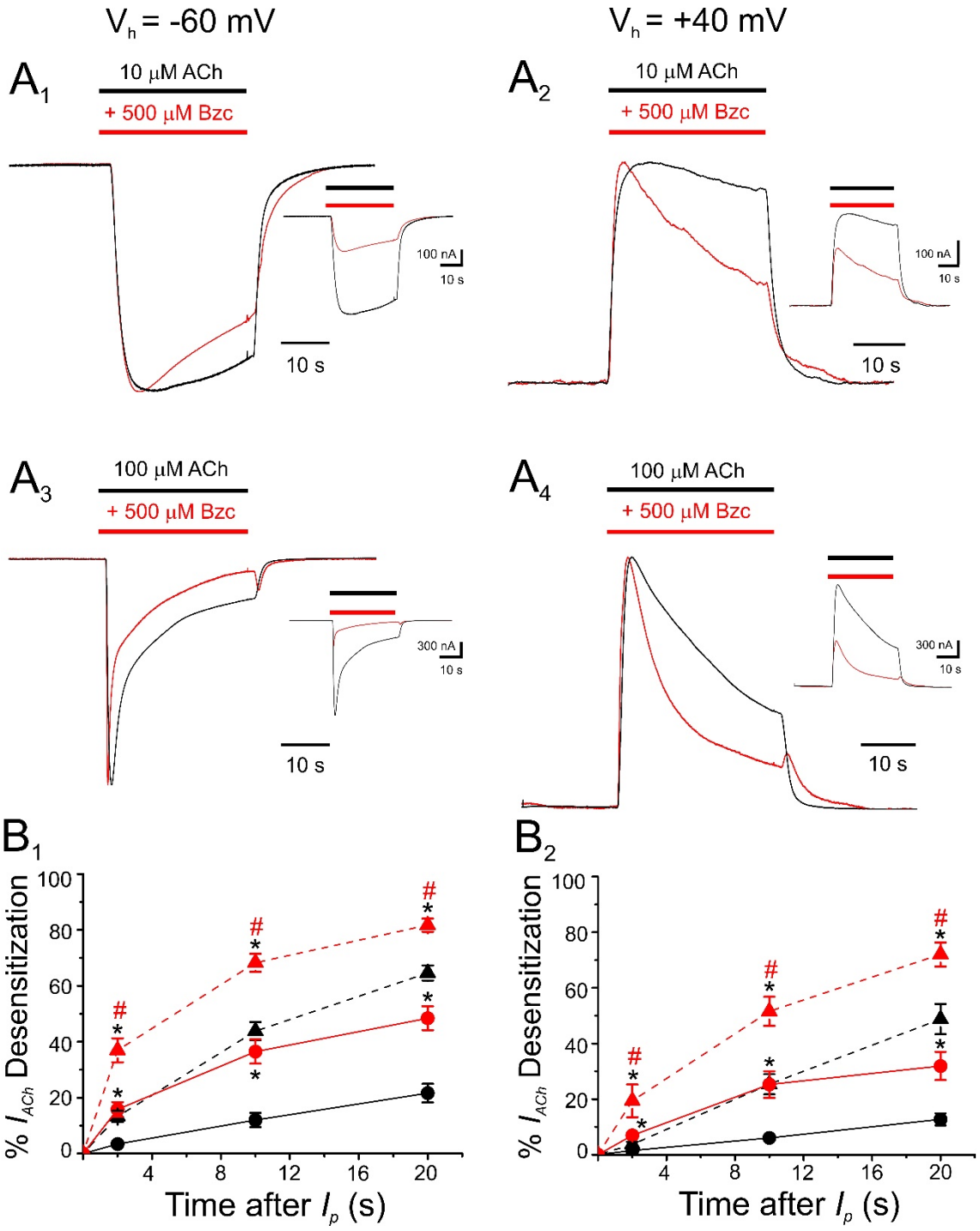


**Figure 7.** *Bzc accelerates $I_{ACh}$ decay.* (**A**) Superimposed $I_{ACh}$s elicited, at -60 mV (**$A_1$**, **$A_3$**) or +40 mV (**$A_2$**, **$A_4$**), by 10 (**$A_1$**, **$A_2$**) or 100 µM ACh (**$A_3$**, **$A_4$**) either alone (black recordings) or with 500 µM Bzc (red recordings). $I_{ACh}$s were scaled to the same $I_p$ amplitude to better compare the differences in $I_{ACh}$ decay. Insets show the corresponding $I_{ACh}$s, before their scaling. (**$B_1$**, **$B_2$**) Plots showing desensitization rates (equation 2) measured at 2, 10 and 20 s after $I_p$ when the holding potential was at either -60 (**$B_1$**) or

+40 mV (**$B_2$**). For 10 µM ACh (circles), each point is the average of 18 (N = 10) and 7 (N = 2) oocytes at -60 and +40 mV, respectively, whereas for 100 µM ACh (triangles) the number of cells was 20 (N = 8) and 5 (N = 1) at those potentials, respectively. Asterisks indicate significant differences among the percentages of $I_{ACh}$ decay in presence of Bzc (red symbols) and their control values (black symbols), at the indicated times ($p < 0.05$, paired *t*-test). Pound signs mean significant differences among the percentages of $I_{ACh}$ desensitization induced by Bzc when it was co-applied with 10 or 100 µM ACh ($p < 0.05$, *t*-test).

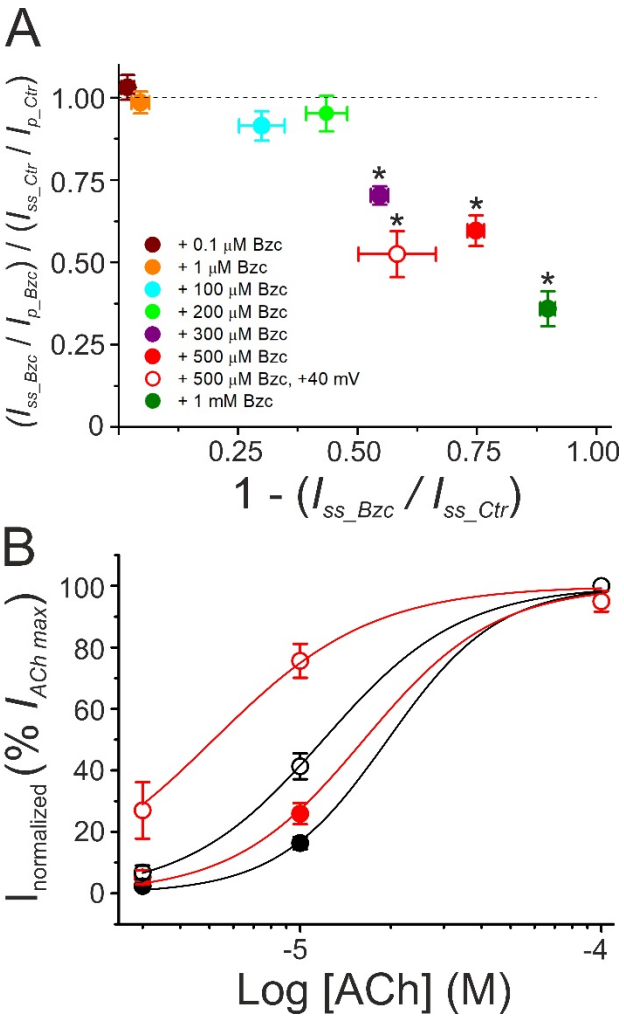


**Figure 8.** *Enhancement of nAChR desensitization depends on Bzc concentration.* **(A)** Relationship between changes in $I_{ACh}$ desensitization (see equation 3) and extent of $I_{ss}$ inhibition when 10 µM ACh was co-applied with Bzc at the indicated concentrations. Holding potential was -60 mV in all cases unless for the open red circle, which was +40 mV. Asterisks indicate significant differences with control desensitization, represented as a discontinuous line (n = 6-17, N = 2-9; $p < 0.05$, one-sample *t*-test). (**B**) ACh concentration-$I_{ACh}$ amplitude relationship in the presence or absence of 500 µM Bzc. $I_p$ (filled circles) and $I_{ss}$ (open circles) elicited by different ACh concentrations either alone (black circles; n = 4-11, N = 2-5) or co-applied with 500 µM Bzc (red circles; the same cells). Data were normalized to the $I_{ACh}$ amplitude elicited by 100 µM ACh at each different protocol and fitted to the Hill equation (equation 4; black and red lines). The $n_H$ values of the fitted curves ranged from 1.92 for the $I_{ss\_Ctr}$ to 2.38 for the $I_{p\_Ctr}$, as expected for nAChR dose-response curves.

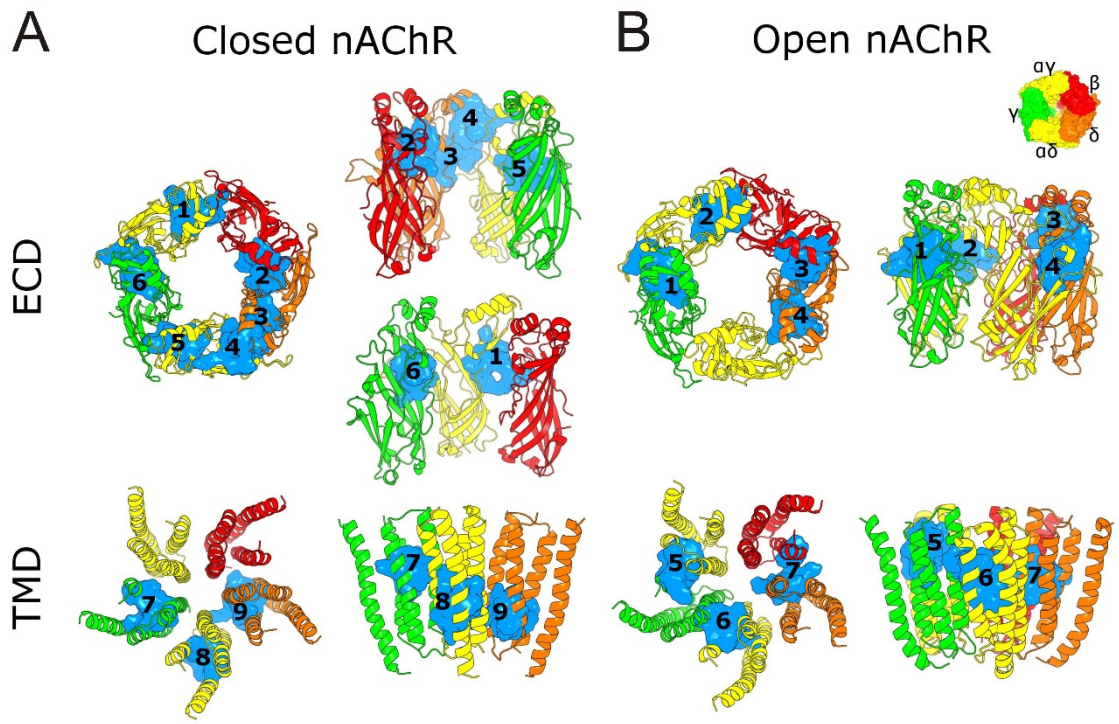


**Figure 9.** *Putative binding sites of Bzc on nAChR in the closed and open states.* **(A)** The main binding sites of Bzc (labelled in cyan) on the refined structure of nAChR in the closed state are indicated by numbers in the extracellular (ECD; uppermost, sites 1-6) and transmembrane (TMD; bottom, sites 7-9) domains. Top (from the synaptic cleft) and side views of the nAChR are shown in the left and in the right of this panel, respectively. **(B)** Major binding sites of Bzc at the ECD (top, sites 1-4) and the TMD (bottom, sites 5-7) of open nAChRs in views similar to those in panel **A**. The inset, in the upper right corner, shows the nAChR subunits with their coding colors.

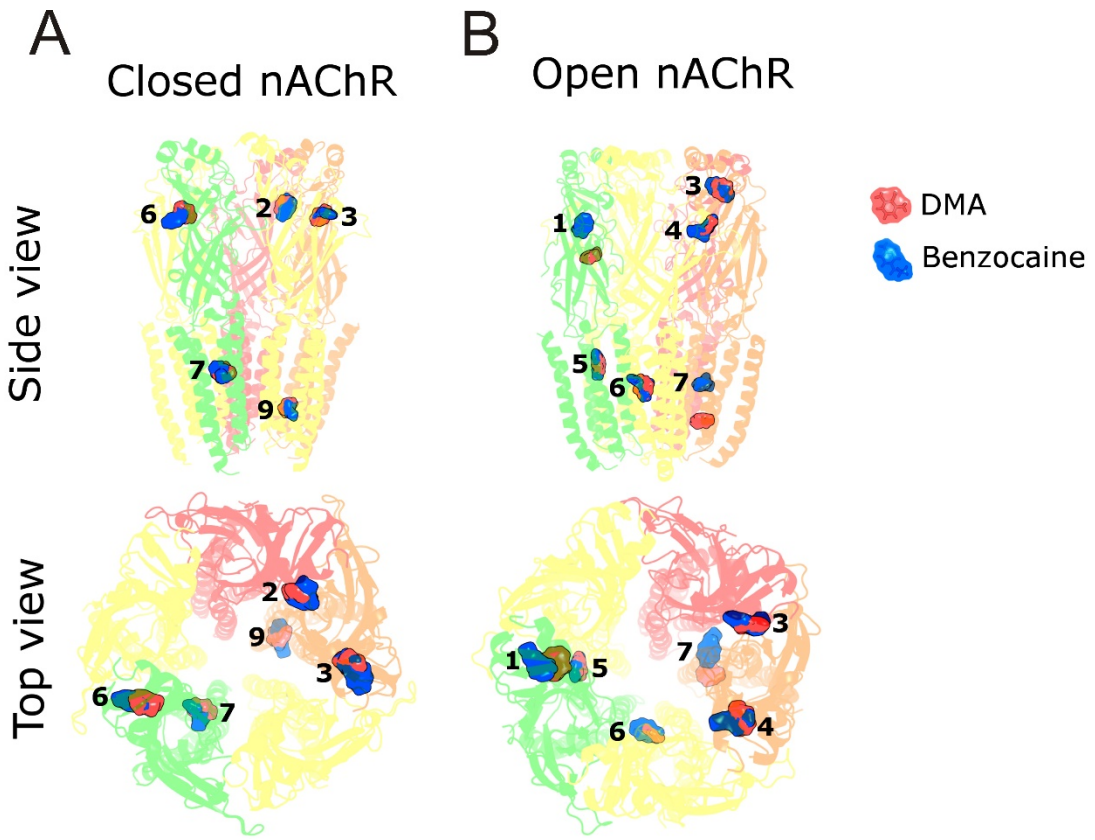


**Figure 10.** *Comparison of Bzc and DMA binding sites on the nAChR in the closed and open conformations.* **(A)** Side view (in the membrane plane; top) and top view (from the synaptic cleft; bottom) of the nAChR in the closed state, showing the most favorable binding sites of Bzc (blue) and DMA (pink) on it. Notice the strong overlap of Bzc and DMA binding sites. The nAChR structure has been made partially transparent to better observe Bzc and DMA molecules. **(B)** Main Bzc and DMA binding sites on nAChR in the open state. Views are similar to those shown in panel **A**. Note the coincidence of their interacting sites on the open nAChR, excluding sites 1 and 7.

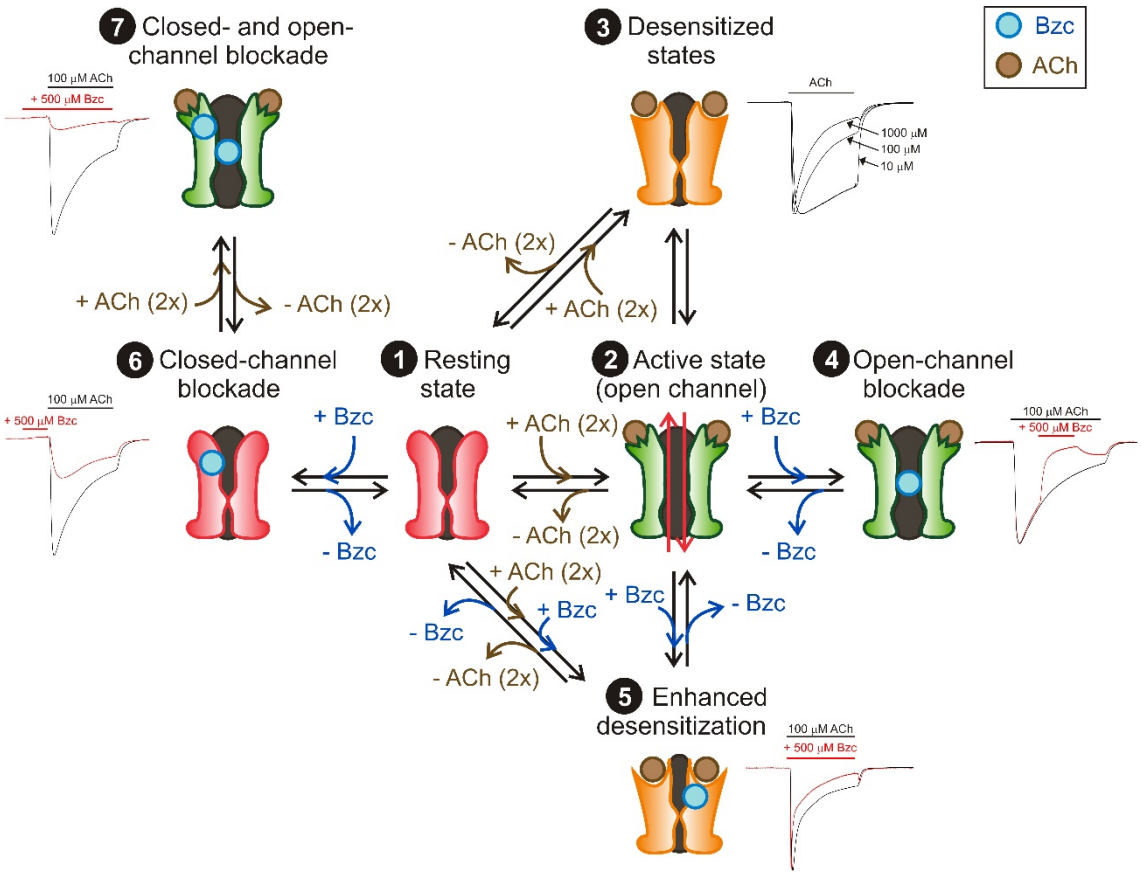


***Figure 11.*** *Model summarizing the effects of Bzc on nAChRs.* This scheme shows the main effects of Bzc on $I_{ACh}$ amplitude and kinetics when binding to different nAChR conformations. Resting nAChR (1) binds ACh and the channel opens (2), being followed by nAChR desensitization, as evidenced by the $I_{ACh}$ decay, which shows a time-course dependent on ACh concentration (3). The presence of Bzc, when the nAChR is in the open state, causes open-channel blockade (4) and enhances desensitization (5). Bzc acting on resting nAChR leads to closed-channel blockade (6) and the subsequent ACh and Bzc co-application results in open- and closed-channel blockade (7). Recordings are the same shown in previous figures. Notice that $I_{ACh}$s elicited by ACh alone are in black, whereas red recordings indicate that Bzc bathed the cell, at the time specified by the red horizontal bar.